

1 *Supporting Information*

2 **Capacitive Removal of Heavy Metal Ions from Wastewater via an**
3 **Electro-Adsorption and Electro-Reaction Coupling Process**

4 Minlin Mao[†], Tingting Yan[†], Junjie Shen[‡], Jianping Zhang[†], and Dengsong Zhang^{†*}

5 [†]*State Key Laboratory of Advanced Special Steel, School of Materials Science and*
6 *Engineering, International Joint Laboratory of Catalytic Chemistry, Research Center*
7 *of Nano Science and Technology, Department of Chemistry, College of Sciences,*
8 *Shanghai University, Shanghai 200444, China.*

9 [‡]*Department of Chemical Engineering, University of Bath, Bath BA2 7AY, UK.*

10 ^{*}*E-mail: dszhang@shu.edu.cn; Tel: +86 21 66137152.*

11
12
13
14 The Supporting Information includes 73 pages, 39 Figures, and 14 Tables.

16	Table of Contents	
17	Figure S1. Schematic illustration of the synthesis route of the W ₁₈ O ₄₉ /Graphene...	S17
18	Figure S2. SEM image of the W ₁₈ O ₄₉ /C.....	S18
19	Figure S3. (a) SEM image, (b-e) EDS mapping, (f) SEM image, (g) TEM image and (h)	
20	HRTEM image of the W ₁₈ O ₄₉ /Graphene.....	S19
21	Figure S4. (a) TEM image, (b, c) HRTEM and (d) SAED patterns of the	
22	W ₁₈ O ₄₉ /Graphene.	S20
23	Figure S5. EDS line scans of the W ₁₈ O ₄₉ /Graphene	S21
24	Figure S6. (a) Nitrogen sorption isotherms of the W ₁₈ O ₄₉ /Graphene and W ₁₈ O ₄₉ /C. (b)	
25	DFT pore size distribution curves of the W ₁₈ O ₄₉ /Graphene and W ₁₈ O ₄₉ /C	S22
26	Figure S7. Dynamic water contact angle analysis of the W ₁₈ O ₄₉ /Graphene, W ₁₈ O ₄₉ /C	
27	materials and AC.....	S23
28	Figure S8. Raman spectra of the W ₁₈ O ₄₉ /Graphene, W ₁₈ O ₄₉ /C and AC.....	S24
29	Figure S9. XPS spectra of the W ₁₈ O ₄₉ /Graphene.....	S25
30	Figure S10. (a) C 1s and (b) O 1s spectra of the W ₁₈ O ₄₉ /Graphene.....	S26
31	Figure S11. Plots of specific capacitance <i>versus</i> scanning rates for W ₁₈ O ₄₉ /Graphene,	
32	W ₁₈ O ₄₉ /C, and AC in a 1000 mg/L NaCl solution.....	S27
33	Figure S12. Charge-discharge curves of W ₁₈ O ₄₉ /Graphene, W ₁₈ O ₄₉ /C, and AC at 0.2	
34	A/g in a 1000 mg/L NaCl solution.....	S28
35	Figure S13. Cycle stability plots of the W ₁₈ O ₄₉ /Graphene electrode at 10 A/g in a 1000	
36	mg/L NaCl solution.....	S29
37	Figure S14. Impedance spectra of W ₁₈ O ₄₉ /Graphene, W ₁₈ O ₄₉ /C, and AC in a 1000 mg/L	

38	NaCl solution.....	S30
39	Figure S15. (a) Charge-discharge curves of the W ₁₈ O ₄₉ /Graphene electrodes in a 1000	
40	mg/L NaCl solution. (b) CV curves of the W ₁₈ O ₄₉ /Graphene electrodes in a 1000 mg/L	
41	NaCl solution.....	S31
42	Figure S16. (a) Charge-discharge curves of the W ₁₈ O ₄₉ /C electrodes in a 1000 mg/L	
43	NaCl solution. (b) CV curves of the W ₁₈ O ₄₉ /C electrodes in a 1000 mg/L NaCl	
44	solution.....	S32
45	Figure S17. (a) Charge-discharge curves of the AC electrodes in a 1000 mg/L NaCl	
46	solution. (b) CV curves of the AC electrodes in a 1000 mg/L NaCl solution.....	S33
47	Figure S18. Plots of salt adsorption capacity of W ₁₈ O ₄₉ /Graphene, W ₁₈ O ₄₉ /C and AC	
48	<i>versus</i> time in a 1000 mg/L NaCl solution at 1.2 V.....	S34
49	Figure S19. Plots of salt adsorption capacity of W ₁₈ O ₄₉ /Graphene <i>versus</i> time in a 1000	
50	mg/L NaCl solution at different voltages.....	S35
51	Figure S20. Plots of salt adsorption capacity of W ₁₈ O ₄₉ /Graphene <i>versus</i> time in	
52	different concentrations of NaCl solutions at 1.2 V.....	S36
53	Figure S21. Plots of salt adsorption rate of W ₁₈ O ₄₉ /Graphene <i>versus</i> time in different	
54	concentrations of NaCl solutions.....	S37
55	Figure S22. Plots of salt adsorption rate of W ₁₈ O ₄₉ /Graphene, W ₁₈ O ₄₉ /C and AC <i>versus</i>	
56	time in a 1000 mg/L NaCl solution at 1.2 V.....	S38
57	Figure S23. Ragone plots of SAR <i>versus</i> SAC of W ₁₈ O ₄₉ /Graphene, W ₁₈ O ₄₉ /C and AC	
58	time in a 1000 mg/L NaCl solution at 1.2 V.....	S39
59	Figure S24. Ragone plots of SAR <i>versus</i> SAC of W ₁₈ O ₄₉ /Graphene in different	

60	concentrations of NaCl solutions.....	S40
61	Figure S25. Plots of charge efficiency of W ₁₈ O ₄₉ /Graphene, W ₁₈ O ₄₉ /C and AC in	
62	different concentrations of NaCl solutions at 1.2 V.....	S41
63	Figure S26. Plots of specific energy consumption of the W ₁₈ O ₄₉ /Graphene, W ₁₈ O ₄₉ /C	
64	and AC electrode <i>versus</i> SAR in a 1000 mg/L NaCl solution at 1.2 V.....	S42
65	Figure S27. Plots of specific energy consumption of the W ₁₈ O ₄₉ /Graphene <i>versus</i> SAR	
66	in different concentrations of NaCl solutions.....	S43
67	Figure S28. Plots of removal efficiency of heavy metal ions with the W ₁₈ O ₄₉ /Graphene	
68	electrode <i>versus</i> different times in the multi-component solution containing all the	
69	seven metal nitrates (10 mg/L for each) and NaCl (100 mg/L) at 1.2 V.....	S44
70	Figure S29. Plots of pH value <i>versus</i> deionization time of W ₁₈ O ₄₉ /Graphene in the	
71	multi-component solution containing all the seven metal nitrates (10 mg/L for each)	
72	and 100 mg/L NaCl at 1.2 V.....	S45
73	Figure S30. XRD patterns of materials after soaking in solutions with different pH	
74	values.....	S46
75	Figure S31. Plots of removal efficiency of heavy metal ion <i>versus</i> pH values in the	
76	multi-component solution containing all the seven metal nitrates (10 mg/L for each)	
77	and 100 mg/L NaCl at 1.2 V.....	S47
78	Figure S32. (a) Plots of absorbance <i>versus</i> aniline concentration. (b) Absorbance curves	
79	in the multi-component solution containing all the seven metal nitrates (10 mg/L for	
80	each) and 100 mg/L NaCl (Line 1). Absorbance curves after aniline adsorption in the	
81	multi-component solution containing all the seven metal nitrates (10 mg/L for each), 20	

82	mg/L aniline and 100 mg/L NaCl (Line 2). Absorbance curves before aniline adsorption	
83	in the multi-component solution containing all the seven metal nitrates (10 mg/L for	
84	each), 20 mg/L aniline and 100 mg/L NaCl (Line 3).....	S48
85	Figure S33. (a) Plots of absorbance <i>versus</i> methyl blue concentration. (b) Absorbance	
86	curves in the multi-component solution containing all the seven metal nitrates (10 mg/L	
87	for each) and 100 mg/L NaCl (Line 1). Absorbance curves after methyl blue adsorption	
88	in the multi-component solution containing all the seven metal nitrates (10 mg/L for	
89	each), 20 mg/L aniline and 100 mg/L NaCl (Line 2). Absorbance curves before methyl	
90	blue adsorption in the multi-component solution containing all the seven metal nitrates	
91	(10 mg/L for each), 20 mg/L methyl blue and 100 mg/L NaCl (Line 3).....	S49
92	Figure S34. CV curves of the W ₁₈ O ₄₉ /Graphene electrodes at 0.2 mV/s in 100 mg/L	
93	CaCl ₂ at a constant voltage of 1.2 V.....	S50
94	Figure S35. XRD patterns of W ₁₈ O ₄₉ /Graphene before and after heavy metal ion	
95	adsorption in single-component metal nitrate solution solutions (metal nitrate (10	
96	mg/L).....	S51
97	Figure S36. XRD patterns of W ₁₈ O ₄₉ /Graphene after Na-adsorbed and Na-desorbed in	
98	100 mg/L NaCl solutions.....	S52
99	Figure S37. XRD patterns of W ₁₈ O ₄₉ /Graphene before and after heavy metal ion	
100	adsorption in the multi-component solution containing all the seven metal nitrates (10	
101	mg/L for each) and 100 mg/L NaCl at a constant voltage of 1.2 V.....	S53
102	Figure S38. (a) CV curves at a scanning rate of 0.2 mV/s in 100 mg/L Pb(NO ₃) ₂	
103	solutions, (b) CV curves at a scanning rate of 0.2 mV/s in 100 mg/L Cr(NO ₃) ₃ solutions,	

104	(c) CV curves at a scanning rate of 0.2 mV/s in 100 mg/L Cd(NO ₃) ₂ solutions, (d) CV	
105	curves at a scanning rate of 0.2 mV/s in 100 mg/L Fe(NO ₃) ₃ solutions, (e) CV curves	
106	at a scanning rate of 0.2 mV/s in 100 mg/L Cu(NO ₃) ₂ solutions, (f) CV curves at a	
107	scanning rate of 0.2 mV/s in 100 mg/L Ni(NO ₃) ₂ solutions, (g) CV curves at a scanning	
108	rate of 0.2 mV/s in 100 mg/L Co(NO ₃) ₂ solutions.....	S54
109	Figure S39. CV curves at a scanning rate of 0.2 mV/s in the multi-component solution	
110	containing all the seven metal nitrates (10 mg/L for each) and 100 mg/L NaCl.....	S55
111	Table S1. Summary of properties of the materials.....	S57
112	Table S2. Summary of relative intensity ratios of all materials in Raman spectra....	S58
113	Table S3. Elemental contents of the synthesized materials determined by XPS	
114	spectra.....	S59
115	Table S4. Comparison of the W ₁₈ O ₄₉ /Graphene materials with the state-of-the-art	
116	materials.....	S60
117	Table S5. Removal efficiency after 120 min of capacitive adsorption in the complex	
118	binary-component solutions [metal nitrate (10 mg/L) and NaCl (100 mg/L)] at 1.2 V by	
119	ICP-OES tested.....	S61
120	Table S6. Removal efficiency after 120 min of capacitive adsorption in the complex	
121	binary-component solutions [metal nitrate (50 mg/L) and NaCl (100 mg/L)] at 1.2 V by	
122	ICP-OES tested.....	S62
123	Table S7. Removal efficiency after 120 min of capacitive adsorption in the multi-	
124	component solution containing all the seven metal nitrates (10 mg/L for each) and 100	
125	mg/L NaCl at a constant voltage of 1.2 V by ICP-OES tested.....	S63

126	Table S8. Removal efficiency after 120 min of capacitive adsorption in the multi-	
127	component solution containing all the seven metal nitrates (10 mg/L for each) and 500	
128	mg/L NaCl at a constant voltage of 1.2 V by ICP-OES tested.....	S64
129	Table S9. Removal efficiency after 120 min of capacitive adsorption in the multi-	
130	component solution containing all the seven metal nitrates (50 mg/L for each) and 100	
131	mg/L NaCl at a constant voltage of 1.2 V by ICP-OES tested.....	S65
132	Table S10. Removal efficiency after 120 min of capacitive adsorption in the multi-	
133	component solution containing all the seven metal nitrates (50 mg/L for each) and 500	
134	mg/L NaCl at a constant voltage of 1.2 V by ICP-OES tested.....	S66
135	Table S11. Heavy metal ions concentration of 20 cycles after 120 min of capacitive	
136	adsorption in the multi-component solution containing all the seven metal nitrates (10	
137	mg/L for each) and 100 mg/L NaCl at a constant voltage of 1.2 V by ICP-OES	
138	tested.....	S67
139	Table S12. Removal efficiency after 120 min of capacitive adsorption in the multi-	
140	component solution containing all the seven metal nitrates (10 mg/L for each) and 100	
141	mg/L CaCl ₂ at a constant voltage of 1.2 V by ICP-OES tested.....	S68
142	Table S13. Removal efficiency after 120 min of capacitive adsorption in the multi-	
143	component solution containing all the seven metal nitrates (10 mg/L for each) and 500	
144	mg/L CaCl ₂ at a constant voltage of 1.2 V by ICP-OES tested.....	S69
145	Table S14. The area corresponding to the peak position of XPS.....	S70
146		

EXPERIMENTAL SECTION

Chemicals.

NaCl (AR, 99%), Pb(NO₃)₂ (AR, 99%), Fe(NO₃)₃ (AR, 99%), Ni(NO₃)₂ (AR, 99%), Co(NO₃)₂ (AR, 99%), Cu(NO₃)₂ (AR, 99%), Cr(NO₃)₃ (AR, 99%), Cd(NO₃)₂ (AR, 99%), (NH₄)₁₀W₁₂O₄₁~xH₂O (AR, 99%), aniline (AR, 99%), methyl blue (AR, 99%), Graphene and CH₃CH₂OH (AR, 99%) were purchased from Sinopharm Chemical Reagent Co. Ltd. Dopamine hydrochloride (AR, 99%) and NH₃·H₂O (28-30%) were obtained from Aladdin Chemistry Co. (Shanghai, China).

Preparation of W₁₈O₄₉/C. W₁₈O₄₉/C samples were synthesized by a simple and reasonable synthesis scheme. 1.2 g of (NH₄)₁₀W₁₂O₄₁~xH₂O was added to 100 mL of tris-buffer solution (pH = 8.5) with a 5-min ultrasonic treatment. The mixed solution was heated and stirred for 30 min at 80°C. 0.4 g of dopamine hydrochloride was added to the above solution and stirred for 120 min. Then 160 mL of CH₃CH₂OH was added to the suspension and stirred for 1 h. Finally, 1.2 mL of NH₃·H₂O was added to the solution, stirred for 120 min, then centrifuged with CH₃CH₂OH, washed, and dried in vacuum for 12 h. The obtained mixtures were carbonized in a nitrogen atmosphere at 750 °C for 4 h (5 °C/min) to obtain W₁₈O₄₉/C.

The tris-buffer solutions preparation: 2 g of trimethylol aminomethane was dissolved in 2 L deionized water, and the pH value of the solution was adjusted to 8.5 by adding 0.1 mol/L hydrochloric acid.

Characterization.

The morphology and structure of the materials were observed by SEM (Sigma-300),

TEM (JEOL JEM-200CX), and HRTEM (FEI Tecnai G2 F20). The structure composition of the materials was explored by X-ray diffractometer (XRD) (X-ray diffractometer, Cu-K- α , 40kV mA). The composition of the sample was analyzed by PHI-5300 X-ray photoelectron spectroscopy (XPS). The Raman spectra were measured with 633 nm laser on HORIBA Science Raman spectrometer. The in-situ Raman measurements were carried out in the voltage range of -0.6 to 0.6 V at a CV scanning rate of 0.2 mV/s using the 633 nm Ar⁺ laser Raman spectrometer (HORIBA Science). The concentration of ions was tested by ICP-OES. The isothermal adsorption-desorption curve of nitrogen was studied via Autosorb-IQ₂. The specific surface area and pore size distribution of the samples were calculated by Brunauer-Emmett-Tell (BET) method and density functional theory (DFT) model, respectively. The wettability of the sample to water was tested by Kruss and DSA100 droplet shape analyzer. The electrochemical performance of the samples was evaluated by an electrochemical workstation (CHI 660E Chenhua, Shanghai). The concentrations of the aniline and methyl blue organic pollutants were detected by UV-vis spectrophotometer

Electrochemical Experiments.

The polytetrafluoroethylene (PTFE), conductive carbon black and the prepared material (5 mg) were fully mixed at a 1:1:8 mass ratio to make the square film, which was cast on graphite film (GF) collector to make asymmetric capacitive deionization experimental working electrode. The CV and galvanostatic charge-discharge (GCD) curves and electrochemical impedance spectroscopy (EIS) were measured in the 1000 mg/L NaCl solutions with a three-electrode system. The calomel electrode and GF serve

as reference electrode and counter electrode, respectively. The capacitance is theoretically calculated by formula (Eq. S1):

$$C = \frac{fIdV}{2mv\Delta V} \quad (S1)$$

C is the capacitance (F/g), I is the response current density (A), m is the mass of active material (g), v is the scanning rate (V/s), and ΔV is the applied voltage window during the CV test (V).

The thickness of electrodes is measured by a Micrometer. T_1 is thickness of electrodes (μm), T_2 is average total thickness (882 μm), T_3 is average current collector (GF) thickness (866 μm). Both the T_2 and T_3 are measured by a micrometer. The thickness of electrodes is calculated by formula (Eq. S2) in theory:

$$T_1 = T_2 - T_3 \quad (S2)$$

The thickness of electrodes for electrochemical test of CV, GCD and EIS is closed to 16 μm .

Batch-Mode Capacitive Removal Experiments.

PTFE, conductive carbon black and the prepared material (40 mg) were fully mixed at a 1:1:8 mass ratio to make the square film, which was cast on graphite film (GF) collector to make asymmetric capacitive removal experimental working electrode. Meanwhile, the symmetric electrode was made by fully mixing polytetrafluoroethylene (PTFE), conductive carbon black and activated carbon (40 mg) according to the mass ratio of 1:1:8. In the comparative experiment, the working electrode and counter electrode of AC electrode were prepared in the same way. The spacer is placed between two electrodes to separate them. 65 mL of NaCl solution circulates through the electrode through the peristaltic pump at 40 mL/min. The conductivity meter (Seven

Multi of Mettler Toledo) is used to monitor the electrical conductivity of NaCl solution.

The pH value of the solution is adjusted by using 0.1 mol L⁻¹ NaOH or HNO₃ solutions to make the range between 4 and 8.

The capacitive removal experiments in NaCl solutions: 65 mL of NaCl solution is circulated through the electrode by a peristaltic pump at the speed of 40 mL/min at 1.2 V for 120 min. The conductivity of NaCl solution was recorded on-line by a conductivity meter (Seven Multi of Mettler Toledo). The salt adsorption capacity (SAC) was calculated by formula (Eq. S3) in theory:

$$SAC = \frac{(C_0 - C)V_b}{m} \quad (S3)$$

SAC stands for the deionized mass specific capacitance, C_0 stands for the initial concentration, and C_t stands for the final concentration, V represents the solution volume (L) and m stands for the quality of electrode material (g).

On the basis of following equation, the salt adsorption rate (SAR, mg g⁻¹ min⁻¹) could be calculated (Eq. S4):^{1, 2}

$$SAR = \frac{SAC}{t} \quad (S4)$$

Where t (min) stands for the desalination time.

The average salt removal rate (ASAR, mg g⁻¹ min⁻¹) is the average of all SAR values obtained throughout the desalination period.^{3, 4}

On the basis of following equation, for constant-voltage, the specific energy consumption (SEC⁻¹, mg J⁻¹) could be calculated (Eq. S5):^{5, 6}

$$SEC^{-1} = \frac{(C_0 - C_t)V}{V_d \int_0^t I dt} \quad (S5)$$

Where I (A) and V_d (V) respectively stand for the time dependent current and applied

voltage.

On the basis of following equation, the charge efficiency (Λ , %) could be calculated

(Eq. S6):⁷

$$\Lambda = \frac{\Gamma \times F}{\Sigma} \quad (\text{S6})$$

Where Γ , F and Σ respectively stand for deionization capacity, Faraday constant and

obtained by integrating current.

On the basis of following equation, the energy consumption (EC, Wh g⁻¹) could be

calculated (Eq. S7):⁸

$$\text{EC} = \frac{V_d \int_0^t I dt}{m} \quad (\text{S7})$$

On the basis of following equation, the water recovery (WR, %) could be calculated

(Eq. S8):^{6,8}

$$\text{WR} = \frac{V_1 t_1}{V_1 t_1 + V_2 t_2} \quad (\text{S8})$$

Where V_1 , t_1 , V_2 and t_2 stand for the volume of initial NaCl solution, the time of NaCl

removed in one cycle, the volume of recuperative initial NaCl solution and the time of

recuperating initial NaCl solution. There is concentration recycle, resulting in $V_1 = V_2$.

On the basis of following equation, the product water-specific Gibbs free energy (Δg ,

J g⁻¹) could be calculated (Eq. S9):⁹

$$\Delta g = 2RT \left\{ \frac{C_0}{WR} \ln \left[\frac{C_0 - C_t WR}{C_0(1 - WR)} \right] - C_t \ln \left[\frac{C_0 - C_t WR}{C_t(1 - WR)} \right] \right\} \quad (\text{S9})$$

Where R and T stand for the ideal gas constant and the absolute temperature.

On the basis of following equation, the energy efficiency (EE, %) could be calculated

(Eq. S10):⁹

$$\text{EE} = \frac{\Delta g}{\text{EC}} \quad (\text{S10})$$

258

259 The removal efficiency (C) was calculated by formula (Eq. S11) in theory:

260
$$C = \frac{C_0 - C_t}{C_t} \quad (\text{S11})$$

261 C stands for the removal efficiency, C_0 stands for the initial concentration, and C_t stands
262 for the final concentration.

263 The capacitive removal experiments in the binary-component heavy metal ions and
264 NaCl solutions: 10 mg/L $\text{Pb}(\text{NO}_3)_2$ and 100 mg/L NaCl solution, 10 mg/L $\text{Fe}(\text{NO}_3)_3$ and
265 100 mg/L NaCl solution, 10 mg/L $\text{Ni}(\text{NO}_3)_2$ and 100 mg/L NaCl solution, 10 mg/L
266 $\text{Cr}(\text{NO}_3)_3$ and 100 mg/L NaCl solution, 10 mg/L $\text{Cd}(\text{NO}_3)_2$ and 100 mg/L NaCl solution,
267 10 mg/L $\text{Co}(\text{NO}_3)_2$ and 100 mg/L NaCl solution, 10 mg/L $\text{Cu}(\text{NO}_3)_2$ solution and 100
268 mg/L NaCl solution, 50 mg/L $\text{Pb}(\text{NO}_3)_2$ and 100 mg/L NaCl solution, 50 mg/L
269 $\text{Fe}(\text{NO}_3)_3$ and 100 mg/L NaCl solution, 50 mg/L $\text{Ni}(\text{NO}_3)_2$ and 100 mg/L NaCl solution,
270 50 mg/L $\text{Cr}(\text{NO}_3)_3$ and 100 mg/L NaCl solution, 50 mg/L $\text{Cd}(\text{NO}_3)_2$ and 100 mg/L NaCl
271 solution, 50 mg/L $\text{Co}(\text{NO}_3)_2$ and 100 mg/L NaCl solution, 50 mg/L $\text{Cu}(\text{NO}_3)_2$ solution
272 and 100 mg/L NaCl solution were configured respectively. Those solutions (65 mL)
273 were circulated through the electrode by a peristaltic pump at the speed of 40 mL/min
274 at 1.2 V for 120 min, respectively. The concentration of heavy metal ions in the solution
275 after 120 min was tested by ICP-OES.

276 The capacitive removal experiments in a variety of single-component heavy metal ion
277 solutions and the multi-component heavy metal ion solution: 10 mg/L $\text{Pb}(\text{NO}_3)_2$, 10
278 mg/L $\text{Fe}(\text{NO}_3)_3$ solution, 10 mg/L $\text{Ni}(\text{NO}_3)_2$ solution, 10 mg/L $\text{Co}(\text{NO}_3)_2$ solution, 10
279 mg/L $\text{Cu}(\text{NO}_3)_2$ solution, 10 mg/L $\text{Cr}(\text{NO}_3)_3$ solution, 10 mg/L $\text{Cd}(\text{NO}_3)_2$ solution; 50

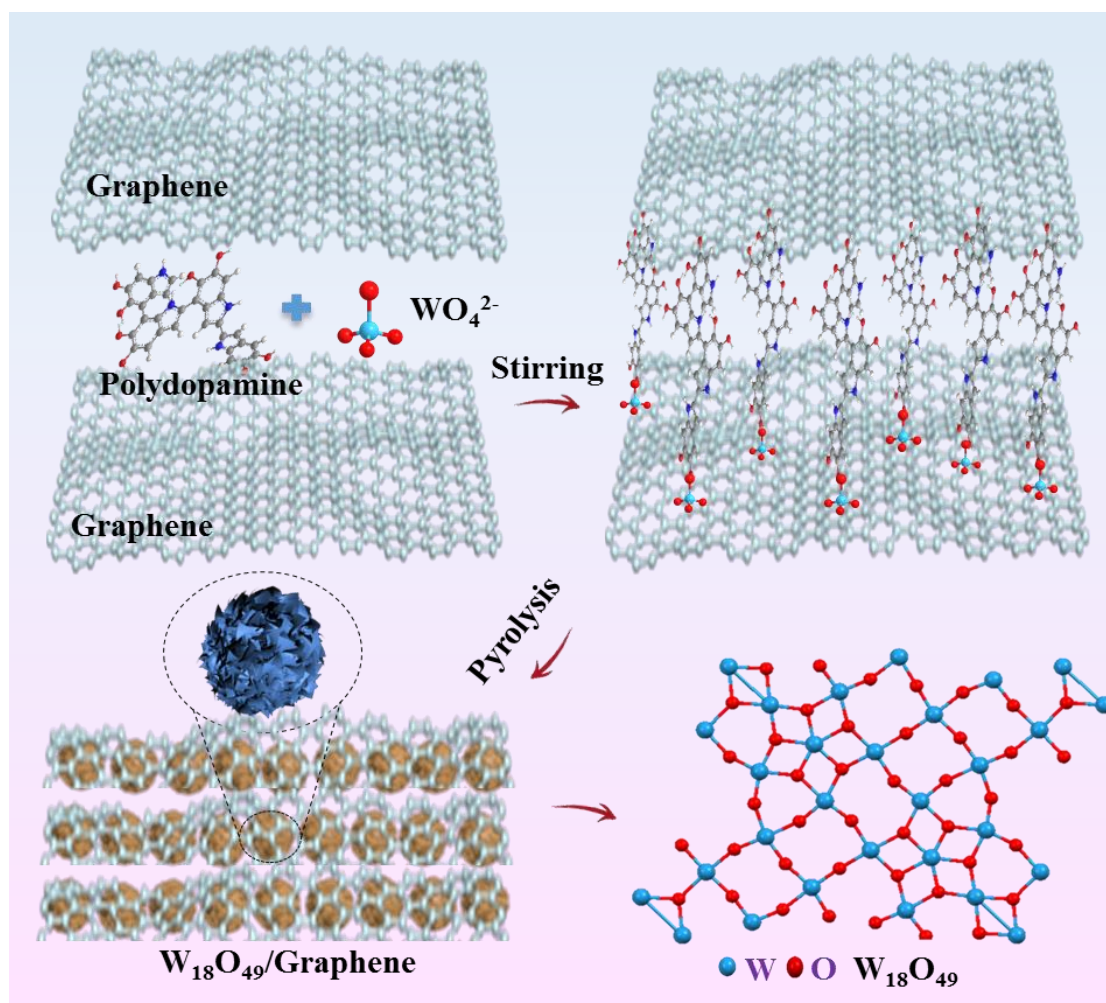
280 mg/L $\text{Pb}(\text{NO}_3)_2$, 50 mg/L $\text{Fe}(\text{NO}_3)_3$ solution, 50 mg/L $\text{Ni}(\text{NO}_3)_2$ solution, 50 mg/L
 281 $\text{Co}(\text{NO}_3)_2$ solution, 50 mg/L $\text{Cu}(\text{NO}_3)_2$ solution, 50 mg/L $\text{Cr}(\text{NO}_3)_3$ solution, 50 mg/L
 282 $\text{Cd}(\text{NO}_3)_2$ solution and 10 mg/L $\text{Pb}(\text{NO}_3)_2$, 10 mg/L $\text{Fe}(\text{NO}_3)_3$, 10 mg/L $\text{Ni}(\text{NO}_3)_2$, 10
 283 mg/L $\text{Co}(\text{NO}_3)_2$, 10 mg/L $\text{Cu}(\text{NO}_3)_2$, 10 mg/L $\text{Cr}(\text{NO}_3)_3$, 10 mg/L $\text{Cd}(\text{NO}_3)_2$, 100 mg/L
 284 NaCl mixed solutions; 10 mg/L $\text{Pb}(\text{NO}_3)_2$, 10 mg/L $\text{Fe}(\text{NO}_3)_3$, 10 mg/L $\text{Ni}(\text{NO}_3)_2$, 10
 285 mg/L $\text{Co}(\text{NO}_3)_2$, 10 mg/L $\text{Cu}(\text{NO}_3)_2$, 10 mg/L $\text{Cr}(\text{NO}_3)_3$, 10 mg/L $\text{Cd}(\text{NO}_3)_2$, 500 mg/L
 286 NaCl mixed solutions; 50 mg/L $\text{Pb}(\text{NO}_3)_2$, 50 mg/L $\text{Fe}(\text{NO}_3)_3$, 50 mg/L $\text{Ni}(\text{NO}_3)_2$, 50
 287 mg/L $\text{Co}(\text{NO}_3)_2$, 50 mg/L $\text{Cu}(\text{NO}_3)_2$, 50 mg/L $\text{Cr}(\text{NO}_3)_3$, 50 mg/L $\text{Cd}(\text{NO}_3)_2$, 100 mg/L
 288 NaCl mixed solutions; 50 mg/L $\text{Pb}(\text{NO}_3)_2$, 50 mg/L $\text{Fe}(\text{NO}_3)_3$, 50 mg/L $\text{Ni}(\text{NO}_3)_2$, 50
 289 mg/L $\text{Co}(\text{NO}_3)_2$, 50 mg/L $\text{Cu}(\text{NO}_3)_2$, 50 mg/L $\text{Cr}(\text{NO}_3)_3$, 50 mg/L $\text{Cd}(\text{NO}_3)_2$, 500 mg/L
 290 NaCl mixed solutions; 10 mg/L $\text{Pb}(\text{NO}_3)_2$, 10 mg/L $\text{Fe}(\text{NO}_3)_3$, 10 mg/L $\text{Ni}(\text{NO}_3)_2$, 10
 291 mg/L $\text{Co}(\text{NO}_3)_2$, 10 mg/L $\text{Cu}(\text{NO}_3)_2$, 10 mg/L $\text{Cr}(\text{NO}_3)_3$, 10 mg/L $\text{Cd}(\text{NO}_3)_2$, 20 mg/L
 292 methyl blue solutions, 100 mg/L NaCl mixed solutions; 10 mg/L $\text{Pb}(\text{NO}_3)_2$, 10 mg/L
 293 $\text{Fe}(\text{NO}_3)_3$, 10 mg/L $\text{Ni}(\text{NO}_3)_2$, 10 mg/L $\text{Co}(\text{NO}_3)_2$, 10 mg/L $\text{Cu}(\text{NO}_3)_2$, 10 mg/L
 294 $\text{Cr}(\text{NO}_3)_3$, 10 mg/L $\text{Cd}(\text{NO}_3)_2$, 20 mg/L aniline solutions, 100 mg/L NaCl mixed
 295 solutions; 10 mg/L $\text{Pb}(\text{NO}_3)_2$, 10 mg/L $\text{Fe}(\text{NO}_3)_3$, 10 mg/L $\text{Ni}(\text{NO}_3)_2$, 10 mg/L
 296 $\text{Co}(\text{NO}_3)_2$, 10 mg/L $\text{Cu}(\text{NO}_3)_2$, 10 mg/L $\text{Cr}(\text{NO}_3)_3$, 10 mg/L $\text{Cd}(\text{NO}_3)_2$, 100 mg/L CaCl_2
 297 mixed solutions; 10 mg/L $\text{Pb}(\text{NO}_3)_2$, 10 mg/L $\text{Fe}(\text{NO}_3)_3$, 10 mg/L $\text{Ni}(\text{NO}_3)_2$, 10 mg/L
 298 $\text{Co}(\text{NO}_3)_2$, 10 mg/L $\text{Cu}(\text{NO}_3)_2$, 10 mg/L $\text{Cr}(\text{NO}_3)_3$, 10 mg/L $\text{Cd}(\text{NO}_3)_2$, 500 mg/L CaCl_2
 299 mixed solutions were configured respectively.

Those solution (65 mL) were circulated through the electrode by a peristaltic pump at the speed of 40 mL/min at 1.2 V for 120 min, respectively. The concentration of heavy metal ions in the solution after 120 min was measured by ICP-OES.

An asymmetric capacitive deionization (CDI) system was used to explore the ability of $W_{18}O_{49}$ /Graphene electrode to adsorb sodium ions in the NaCl solutions. In the asymmetric capacitive deionization system, $W_{18}O_{49}$ /Graphene and $W_{18}O_{49}$ /C materials were used as the cathode and AC as the anode. In contrast, AC was used as both the cathode and the anode in a symmetric capacitive deionization system. The asymmetric $W_{18}O_{49}$ /Graphene||AC, $W_{18}O_{49}$ /C||AC and the symmetric AC||AC were first tested in a 1000 mg/L NaCl solution at 1.2 V. The results show that $W_{18}O_{49}$ /Graphene has the largest salt adsorption capacity (SAC) which is up to 78 mg/g (Figure S18). This is because the layered structure of $W_{18}O_{49}$ /Graphene can provide a fast channel for ion transfer from the electrolyte, which is helpful to improve the ion implantation ability. The SAC of $W_{18}O_{49}$ /Graphene electrode has reached a higher level compared with many reported values in literature (Table S4). Furthermore, the desalination ability of $W_{18}O_{49}$ /Graphene electrode is studied at different voltages in the 1000 mg/L NaCl solution (Figure S19). The results show that the $W_{18}O_{49}$ /Graphene electrode can obtain a higher SAC at 1.2 V. Meanwhile, the SAC of $W_{18}O_{49}$ /Graphene electrode increases with the increase of NaCl concentration (Figure S20). In addition, the salt adsorption rate is also used to measure the desalination performance of the electrode in different concentration NaCl solutions. The $W_{18}O_{49}$ /Graphene electrode has a higher salt adsorption rate than other electrodes in the 1000 mg/L NaCl solutions (Figure S21-22).

322 The corresponding maximum salt adsorption rate of the $W_{18}O_{49}$ /Graphene electrode is
323 0.22 mg/g/s in a 1000 mg/L NaCl solution at a constant voltage of 1.2 V. At the same
324 time, the average salt adsorption rate is 0.032 mg/g/s. The high desalting ability and
325 fast salt adsorption rate are mainly attributed to the electro-adsorption behavior of the
326 electrode. From the Ragone curve, it can be seen that the increase of concentration will
327 make the curve shift to the upper right corner, which indicates that salt adsorption rate
328 (SAR) and SAC increase with the increase of concentration (Figure S23-24). The
329 $W_{18}O_{49}$ /Graphene electrode also showed the higher charge efficiency than other
330 electrodes in different NaCl solutions at a constant voltage of 1.2 V (Figure S25). The
331 charge efficiency of $W_{18}O_{49}$ /Graphene electrode can be maintained at 84%~90% in
332 100~1000 mg/L NaCl solutions at a constant voltage of 1.2 V. The specific energy
333 consumption (SEC^{-1}) of the electrodes was observed. It displayed an intrinsic trade-off
334 between SEC^{-1} and SAR. The $W_{18}O_{49}$ /Graphene electrode had the highest salt
335 adsorption rate in the same energy consumption in the 1000 mg/L NaCl solution,
336 indicating that the electrode could absorb more ions at the same energy consumption
337 (Figure S26-27). At the same time, the energy consumption of $W_{18}O_{49}$ /Graphene
338 electrode is reduced to 0.34 Wh g^{-1} in a 1000 mg/L NaCl solution at a constant voltage
339 of 1.2 V, which is lower than that of traditional capacitive deionization (0.37-3.8 Wh g^{-1})¹⁰. The energy efficiency of the $W_{18}O_{49}$ /Graphene can also reach 30% in a 1000 mg/L
340 NaCl solution at a constant voltage of 1.2 V.

342



343

344

Figure S1. Schematic illustration of the synthesis route of the $W_{18}O_{49}/Graphene$.

345

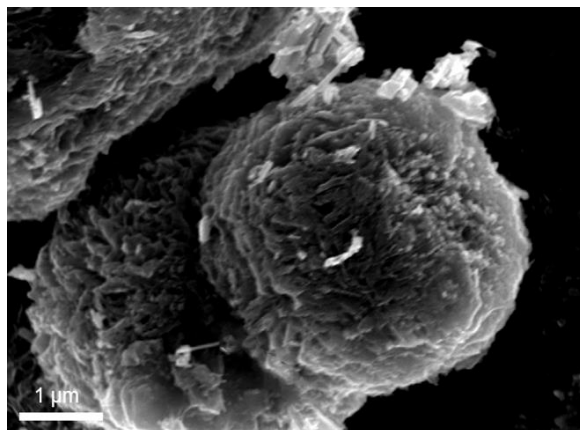
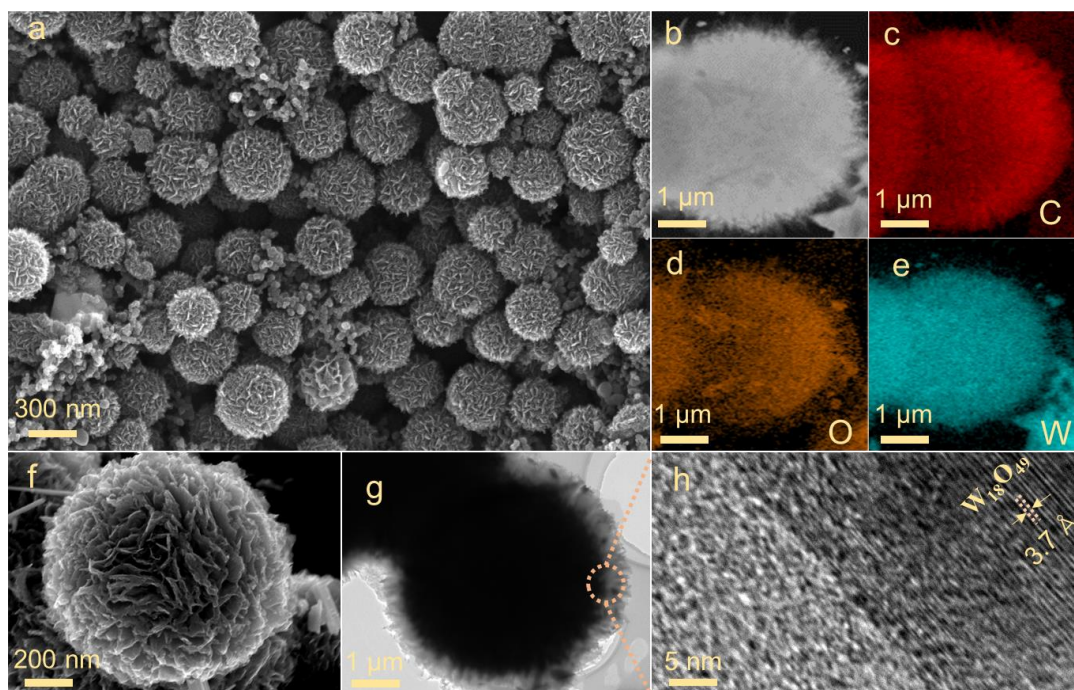


Figure S2. SEM image of the $W_{18}O_{49}/C$.

349



350

351 Figure S3. (a) SEM image, (b-e) EDS mapping, (f) SEM image, (g) TEM image and (h)

352 HRTEM image of the $W_{18}O_{49}$ /Graphene.

353

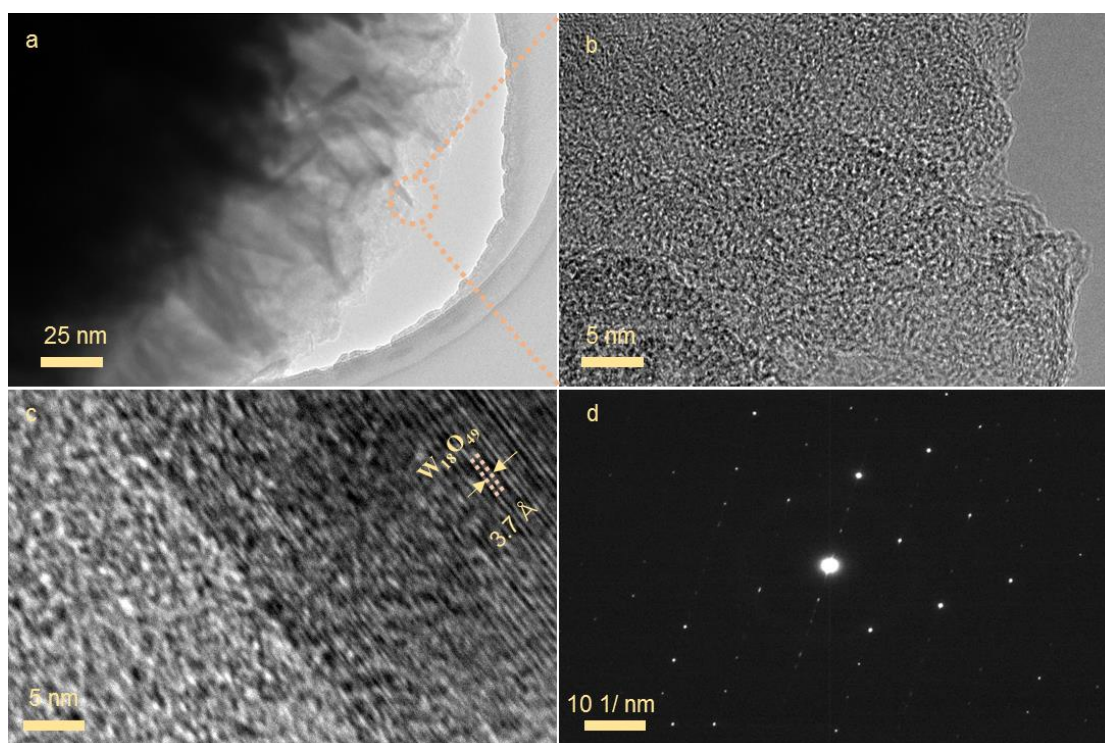


Figure S4. (a) TEM image, (b, c) HRTEM and (d) SAED patterns of the $W_{18}O_{49}/\text{Graphene}$.

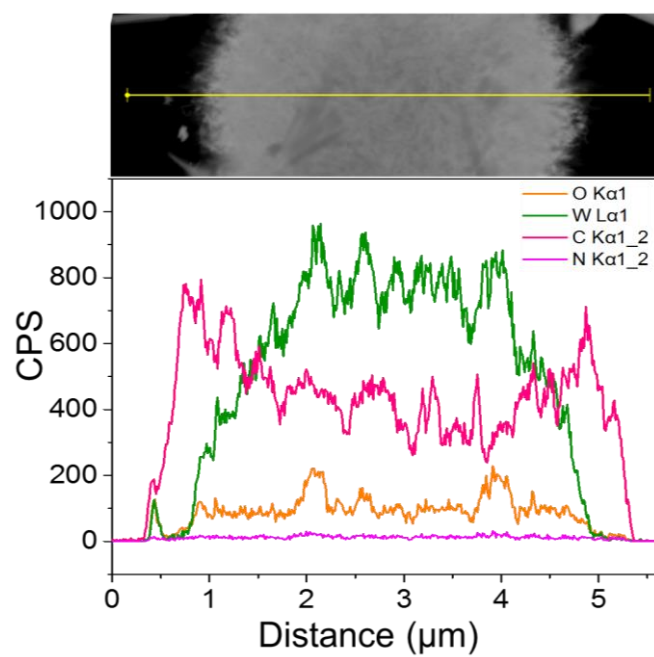


Figure S5. EDS line scans of the $W_{18}O_{49}$ /Graphene.

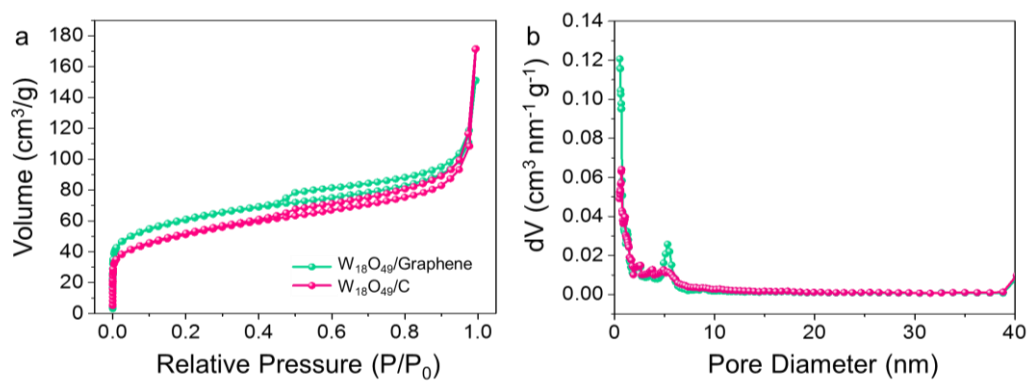


Figure S6. (a) Nitrogen sorption isotherms of the W₁₈O₄₉/Graphene and W₁₈O₄₉/C. (b) DFT pore size distribution curves of the W₁₈O₄₉/Graphene and W₁₈O₄₉/C.

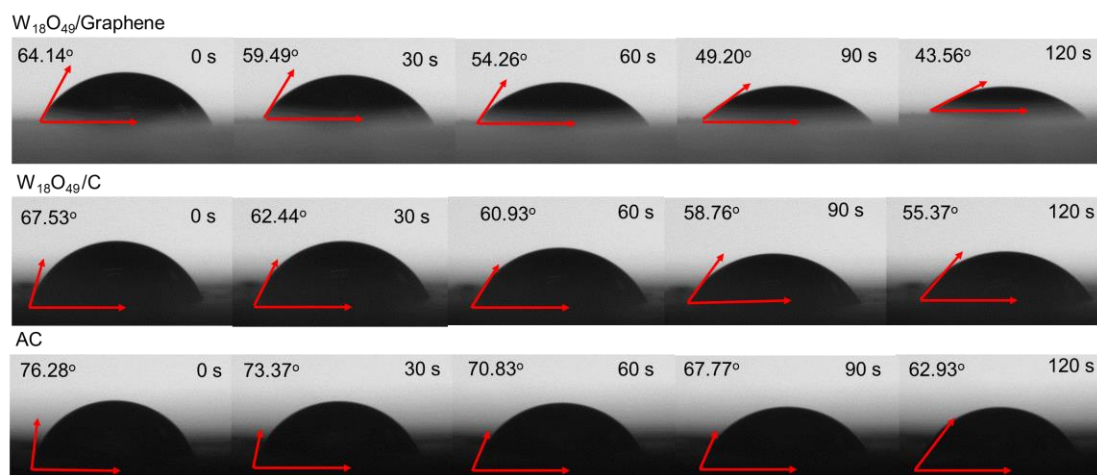
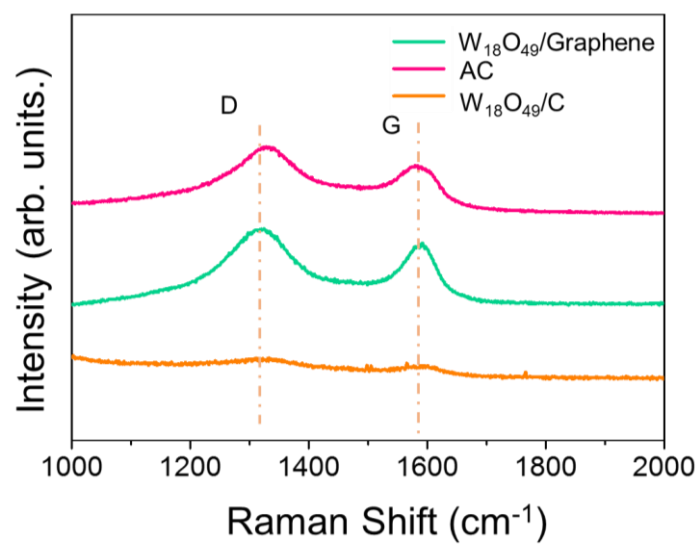


Figure S7. Dynamic water contact angle analysis of the $W_{18}O_{49}/\text{Graphene}$, $W_{18}O_{49}/C$ and AC.

369

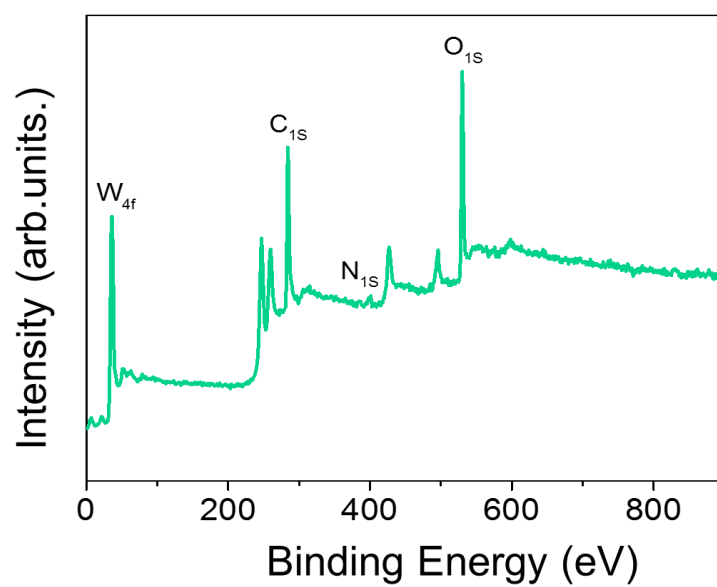


370

371 Figure S8. Raman spectra of the W₁₈O₄₉/Graphene, W₁₈O₄₉/C and AC.

372

373



374

375

Figure S9. XPS spectra of the W₁₈O₄₉/Graphene.

376

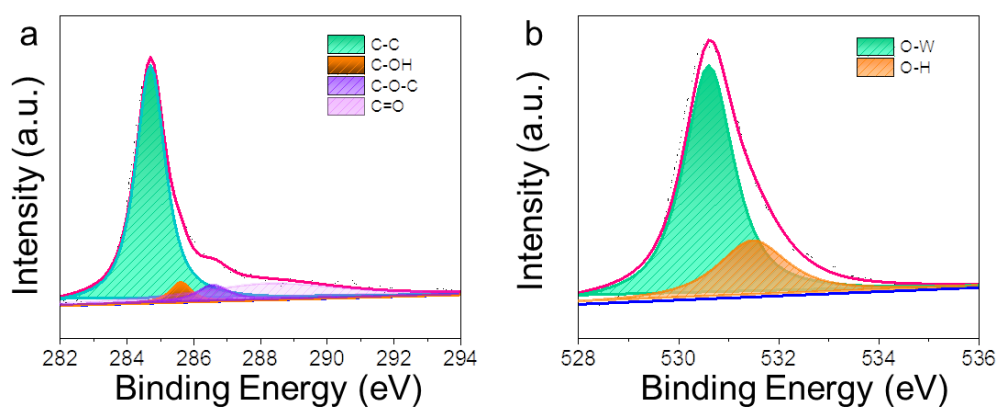
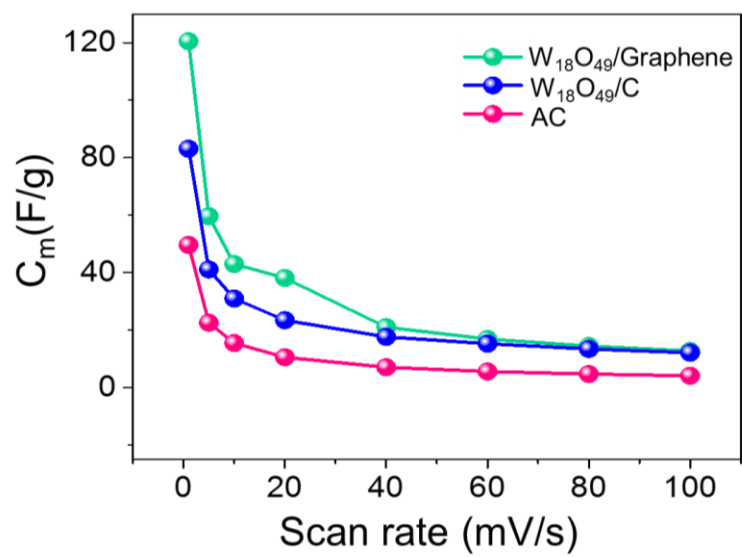


Figure S10. (a) C 1s and (b) O 1s spectra of the $W_{18}O_{49}$ /Graphene.

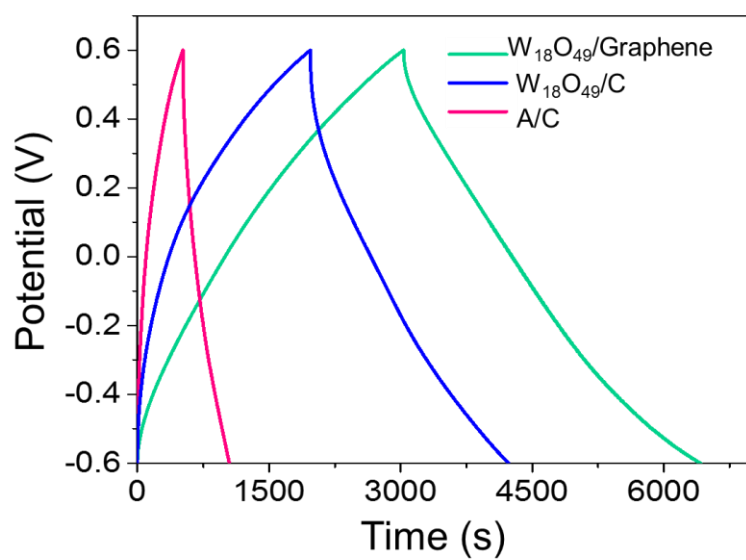


380

381 Figure S11. Plots of specific capacitance *versus* scanning rates for $W_{18}O_{49}/\text{Graphene}$,

382 $W_{18}O_{49}/C$, and AC in a 1000 mg/L NaCl solution.

383

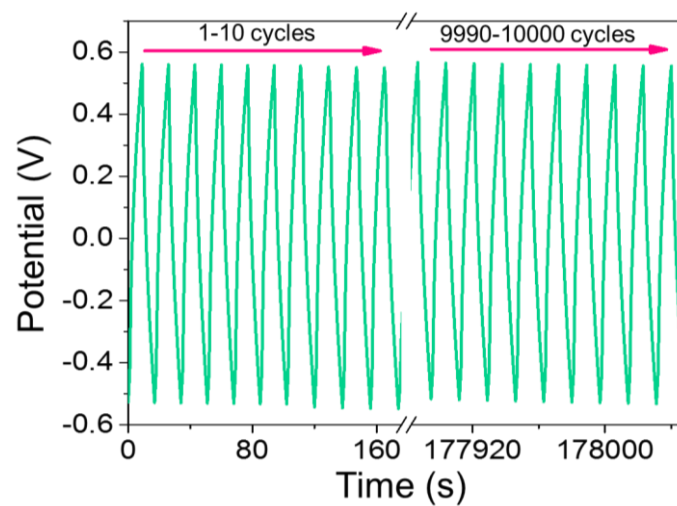


384

385 Figure S12. Charge-discharge curves of $W_{18}O_{49}/\text{Graphene}$, $W_{18}O_{49}/C$, and AC at 0.2

386 A/g in a 1000 mg/L NaCl solution.

387



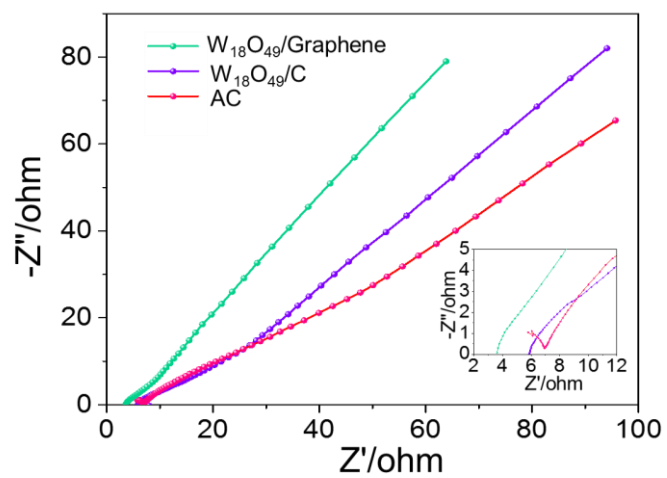
388

389 Figure S13. Cycle stability plots of the $W_{18}O_{49}$ /Graphene electrode at 10 A/g in a 1000

390 mg/L NaCl solution.

391

392

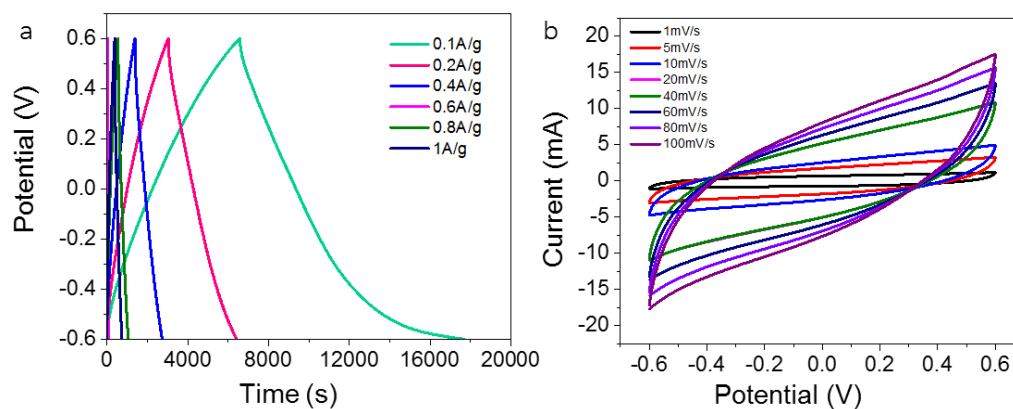


393

394 Figure S14. Impedance spectra of W₁₈O₄₉/Graphene, W₁₈O₄₉/C, and AC in a 1000 mg/L

395 NaCl solution.

396



397

398 Figure S15. (a) Charge-discharge curves of the $W_{18}O_{49}$ /Graphene electrodes in a 1000

399 mg/L NaCl solution. (b) CV curves of the $W_{18}O_{49}$ /Graphene electrodes in a 1000 mg/L

400 NaCl solution.

401

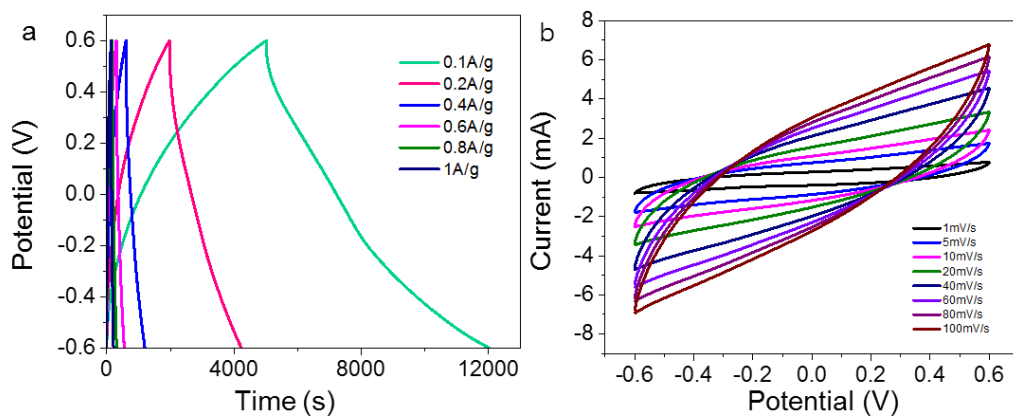


Figure S16. (a) Charge-discharge curves of the $W_{18}O_{49}/C$ electrodes in a 1000 mg/L NaCl solution. (b) CV curves of the $W_{18}O_{49}/C$ electrodes in a 1000 mg/L NaCl solution.

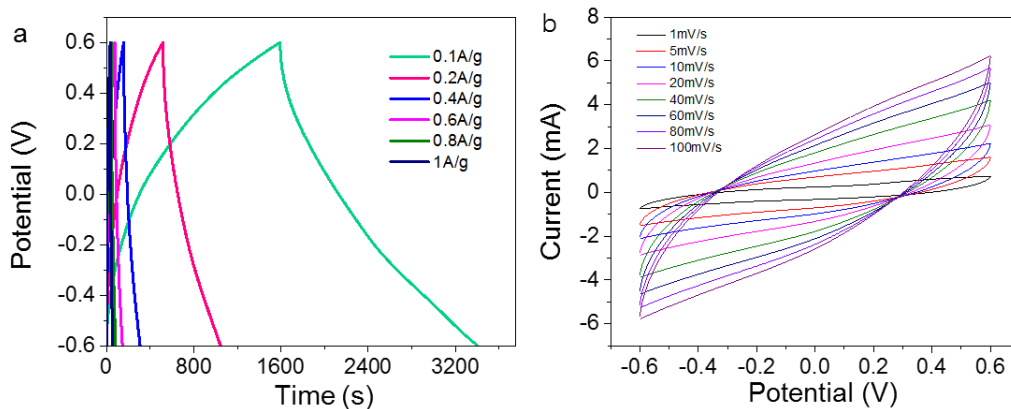
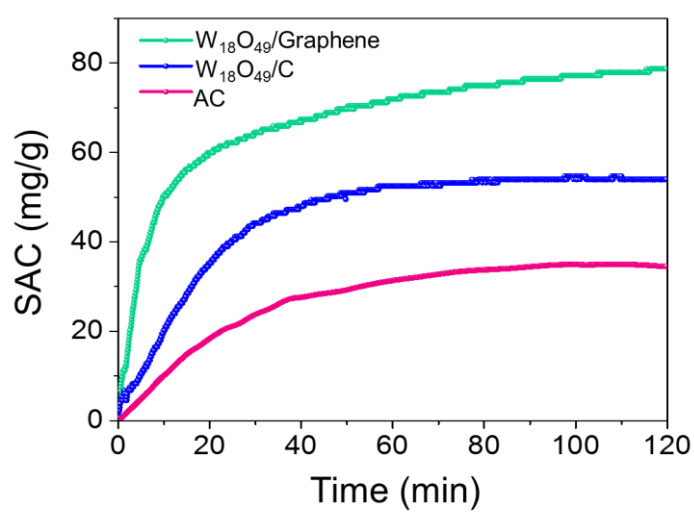


Figure S17. (a) Charge-discharge curves of the AC electrodes in a 1000 mg/L NaCl solution. (b) CV curves of the AC electrodes in a 1000 mg/L NaCl solution.



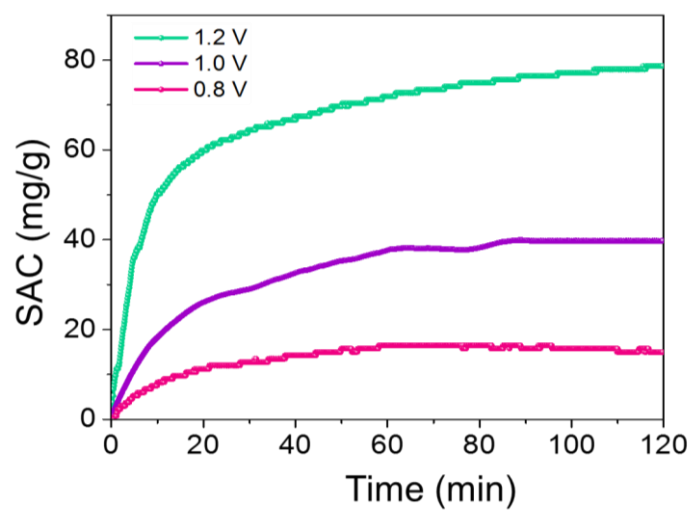
410

411 Figure S18. Plots of salt adsorption capacity of $W_{18}O_{49}/\text{Graphene}$, $W_{18}O_{49}/C$ and AC

412 *versus* time in a 1000 mg/L NaCl solution at 1.2 V.

413

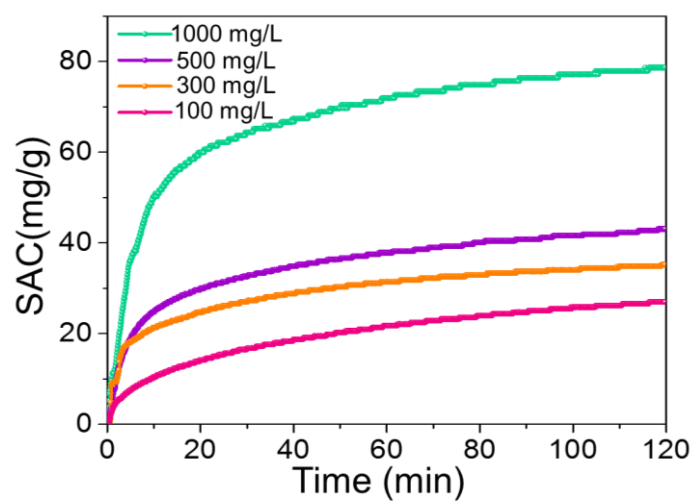
414



415

416 Figure S19. Plots of salt adsorption capacity of $W_{18}O_{49}/\text{Graphene}$ *versus* time in a 1000
417 mg/L NaCl solution at different voltages.

418

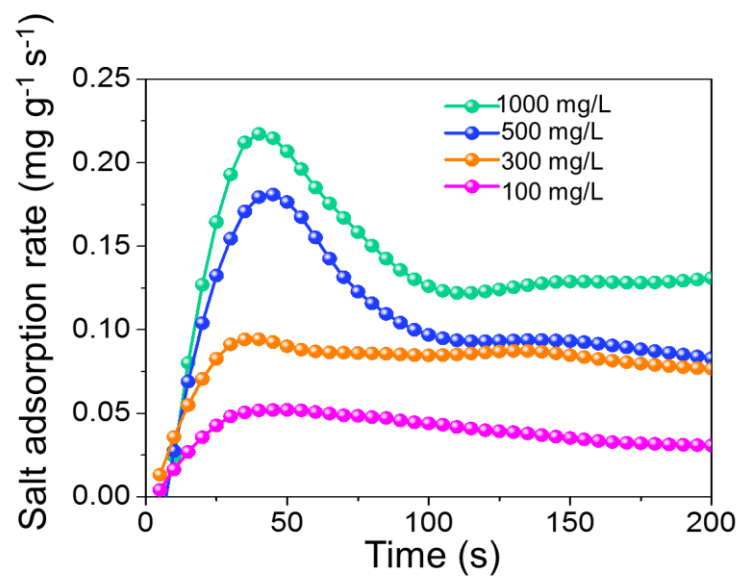


419

420 Figure S20. Plots of salt adsorption capacity of $W_{18}O_{49}/\text{Graphene}$ *versus* time in

421 different concentrations of NaCl solutions at 1.2 V.

422



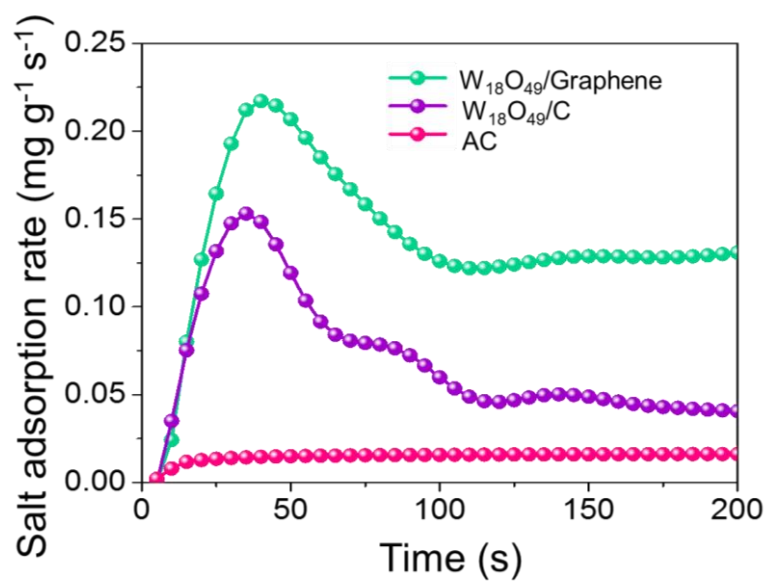
423

424 Figure S21. Plots of salt adsorption rate of W₁₈O₄₉/Graphene *versus* time in different

425 concentrations of NaCl solutions.

426

427



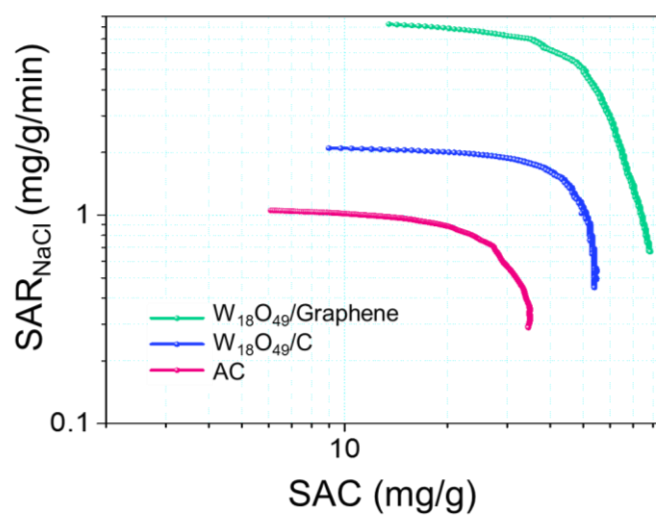
428

429 Figure S22. Plots of salt adsorption rate of W₁₈O₄₉/Graphene, W₁₈O₄₉/C and AC *versus*

430 time in a 1000 mg/L NaCl solution at 1.2 V.

431

432

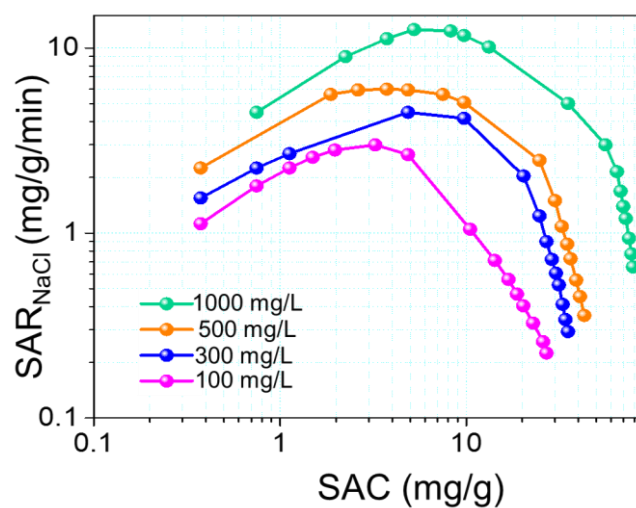


433

434 Figure S23. Ragone plots of SAR *versus* SAC of W₁₈O₄₉/Graphene, W₁₈O₄₉/C and AC

435 time in a 1000 mg/L NaCl solution at 1.2 V.

436

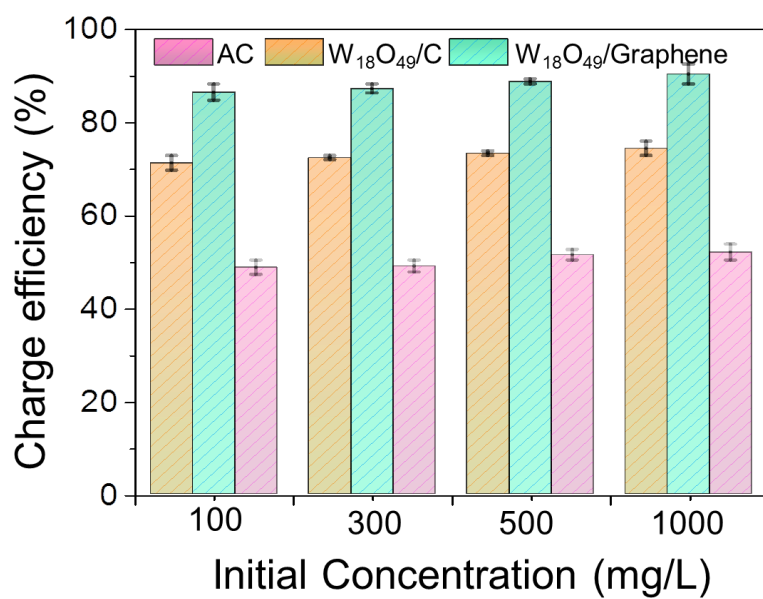


437

438 Figure S24. Ragone plots of SAR versus SAC of $W_{18}O_{49}/Graphene$ in different

439 concentrations of NaCl solutions.

440



441

442 Figure S25. Plots of charge efficiency of $W_{18}O_{49}/\text{Graphene}$, $W_{18}O_{49}/C$ and AC in

443 different concentrations of NaCl solutions at 1.2 V.

444

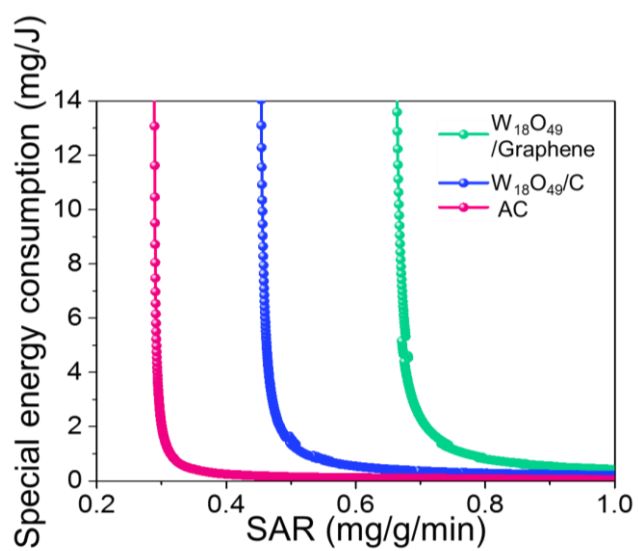
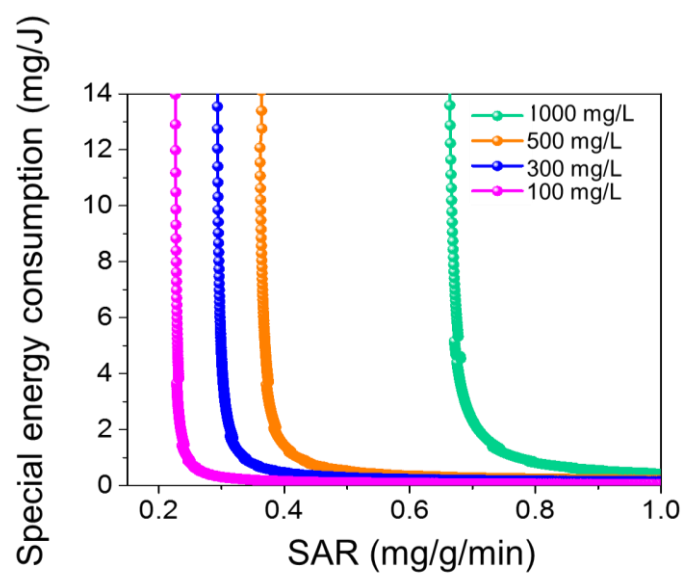


Figure S26. Plots of specific energy consumption of the W₁₈O₄₉/Graphene, W₁₈O₄₉/C and AC electrode *versus* SAR in a 1000 mg/L NaCl solution at 1.2 V.



449

450 Figure S27. Plots of specific energy consumption of the $W_{18}O_{49}$ /Graphene *versus* SAR

451 in different concentrations of NaCl solutions.

452

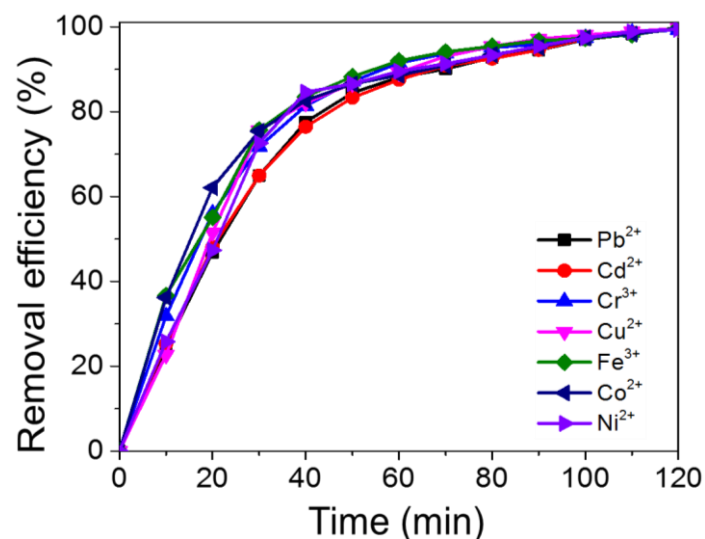
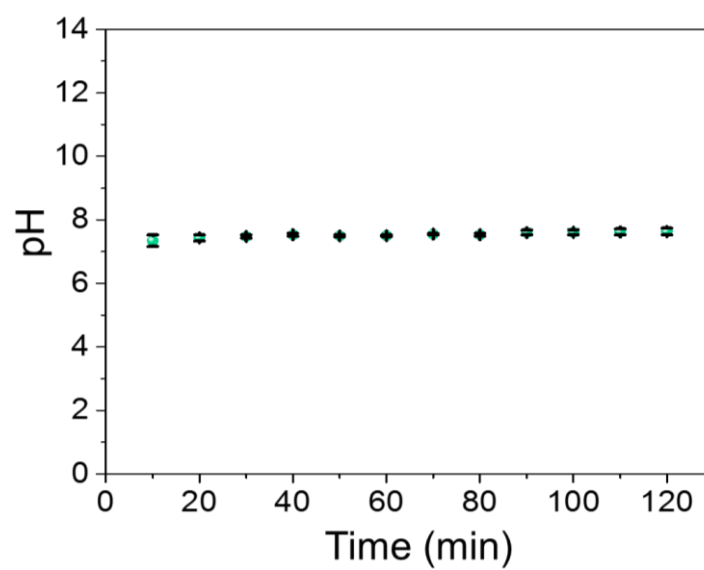


Figure S28. Plots of removal efficiency of heavy metal ions with the $W_{18}O_{49}$ /Graphene electrode *versus* different times in the multi-component solution containing all the seven metal nitrates (10 mg/L for each) and NaCl (100 mg/L) at 1.2 V.



458

459 Figure S29. Plot of pH value *versus* deionization time of $W_{18}O_{49}$ /Graphene in the multi-

460 component solution containing all the seven metal nitrates (10 mg/L for each) and 100

461 mg/L NaCl at 1.2 V.

462

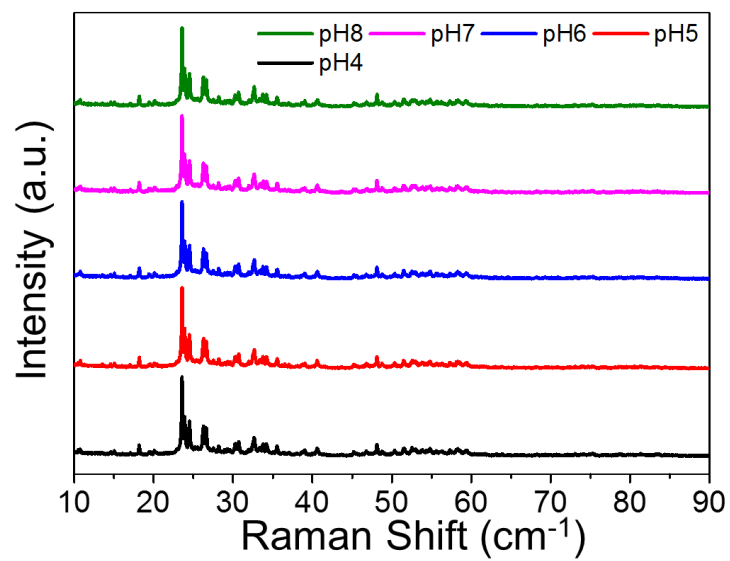
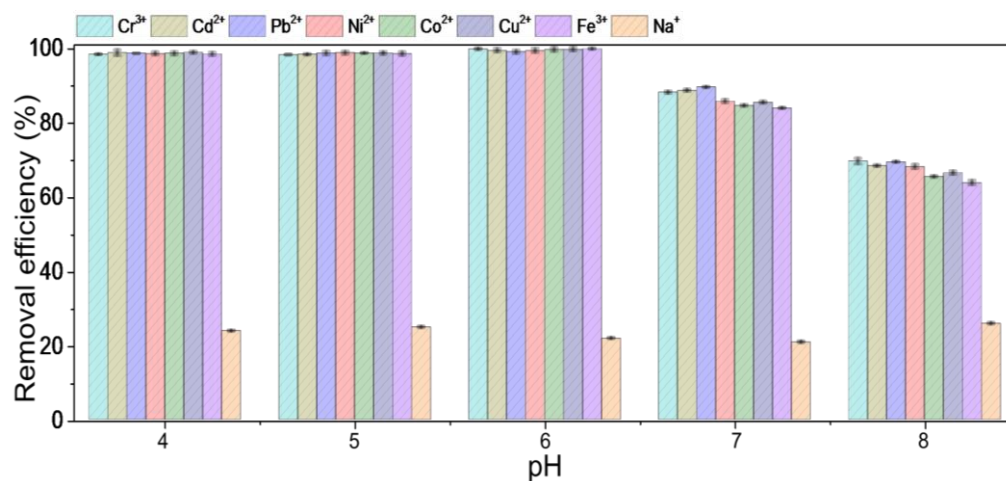


Figure S30. XRD patterns of materials after soaking in solutions with different pH values.



467 Figure S31. Plots of removal efficiency of heavy metal ion *versus* pH values in the
 468 multi-component solution containing all the seven metal nitrates (10 mg/L for each)
 469 and 100 mg/L NaCl at 1.2 V.
 470

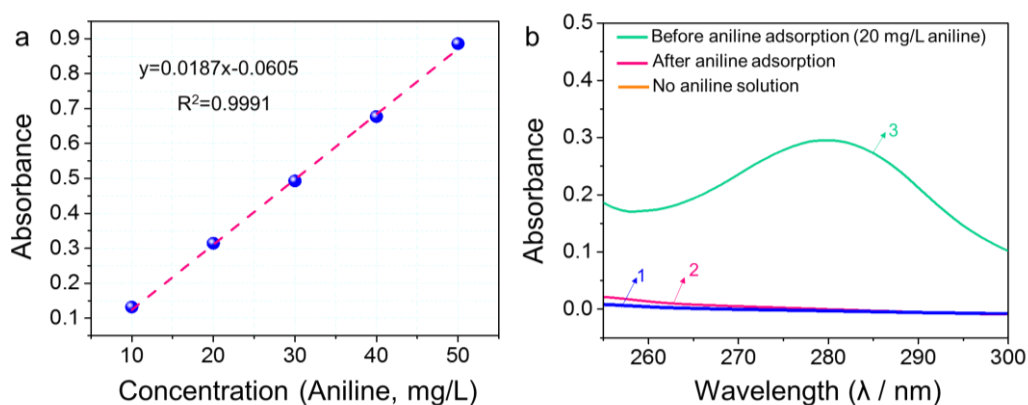


Figure S32. (a) Plots of absorbance *versus* aniline concentration. (b) Absorbance curves in the multi-component solution containing all the seven metal nitrates (10 mg/L for each) and 100 mg/L NaCl (Line 1). Absorbance curves after aniline adsorption in the multi-component solution containing all the seven metal nitrates (10 mg/L for each), 20 mg/L aniline and 100 mg/L NaCl (Line 2). Absorbance curves before aniline adsorption in the multi-component solution containing all the seven metal nitrates (10 mg/L for each), 20 mg/L aniline and 100 mg/L NaCl (Line 3).

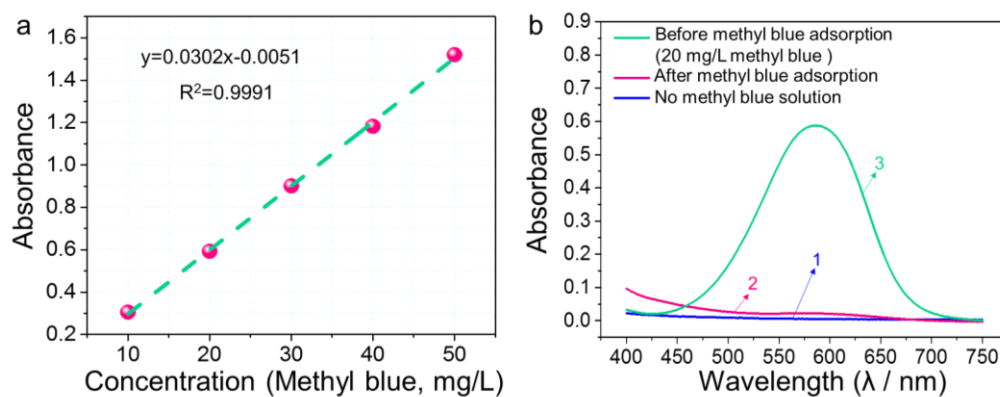
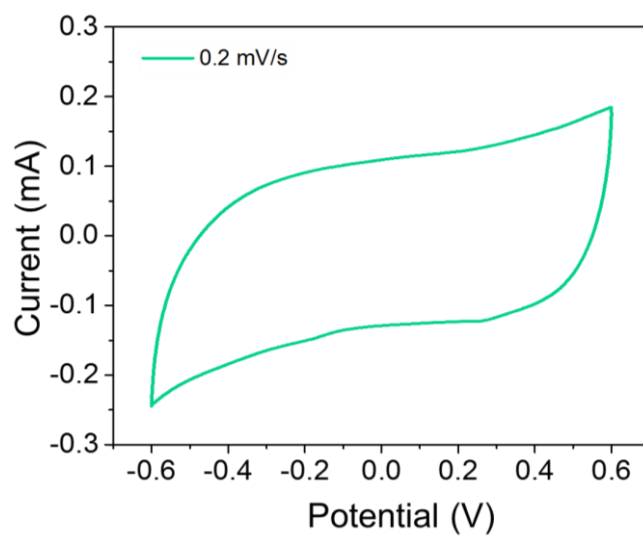


Figure S33. (a) Plots of absorbance *versus* methyl blue concentration. (b) Absorbance curves in the multi-component solution containing all the seven metal nitrates (10 mg/L for each) and 100 mg/L NaCl (Line 1). Absorbance curves after methyl blue adsorption in the multi-component solution containing all the seven metal nitrates (10 mg/L for each), 20 mg/L aniline and 100 mg/L NaCl (Line 2). Absorbance curves before methyl blue adsorption in the multi-component solution containing all the seven metal nitrates (10 mg/L for each), 20 mg/L methyl blue and 100 mg/L NaCl (Line 3).



489

490 Figure S34. CV curves of the $\text{W}_{18}\text{O}_{49}$ /Graphene electrodes at 0.2 mV/s in 100 mg/L

491 CaCl_2 at a constant voltage of 1.2 V.

492

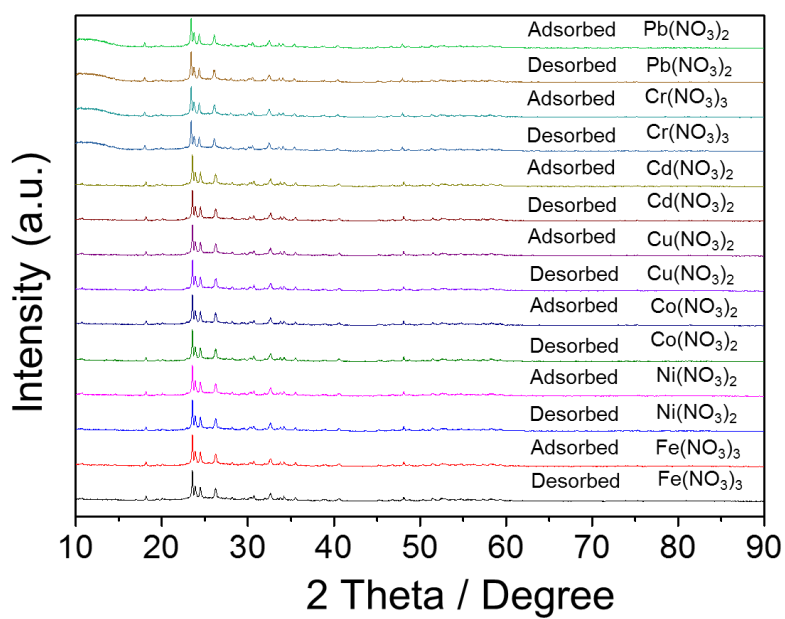
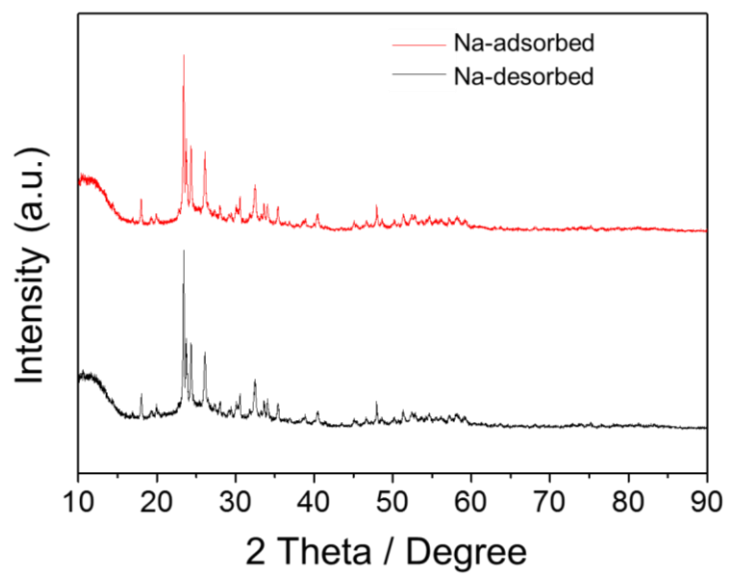


Figure S35. XRD patterns of $W_{18}O_{49}$ /Graphene before and after heavy metal ion adsorption in single-component metal nitrate solution solutions (metal nitrate (10 mg/L)).

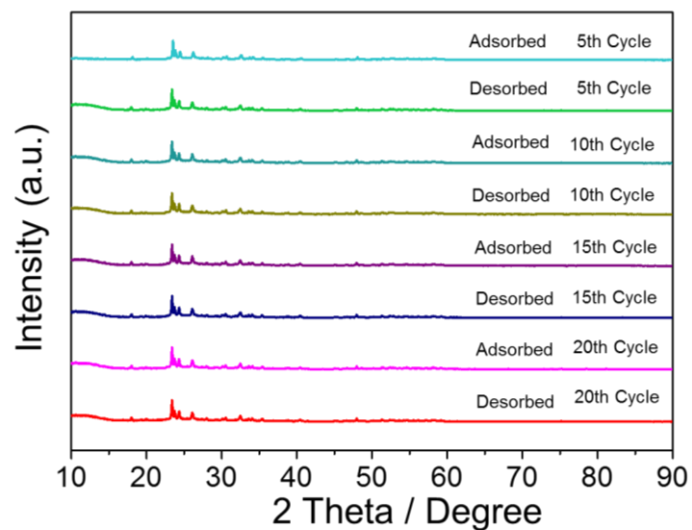


497

498 Figure S36. XRD patterns of $W_{18}O_{49}$ /Graphene after Na-adsorbed and Na-desorbed in

499 100 mg/L NaCl solutions.

500



501

502 Figure S37. XRD patterns of $W_{18}O_{49}$ /Graphene before and after heavy metal ion

503 adsorption in the multi-component solution containing all the seven metal nitrates (10

504 mg/L for each) and 100 mg/L NaCl at a constant voltage of 1.2 V.

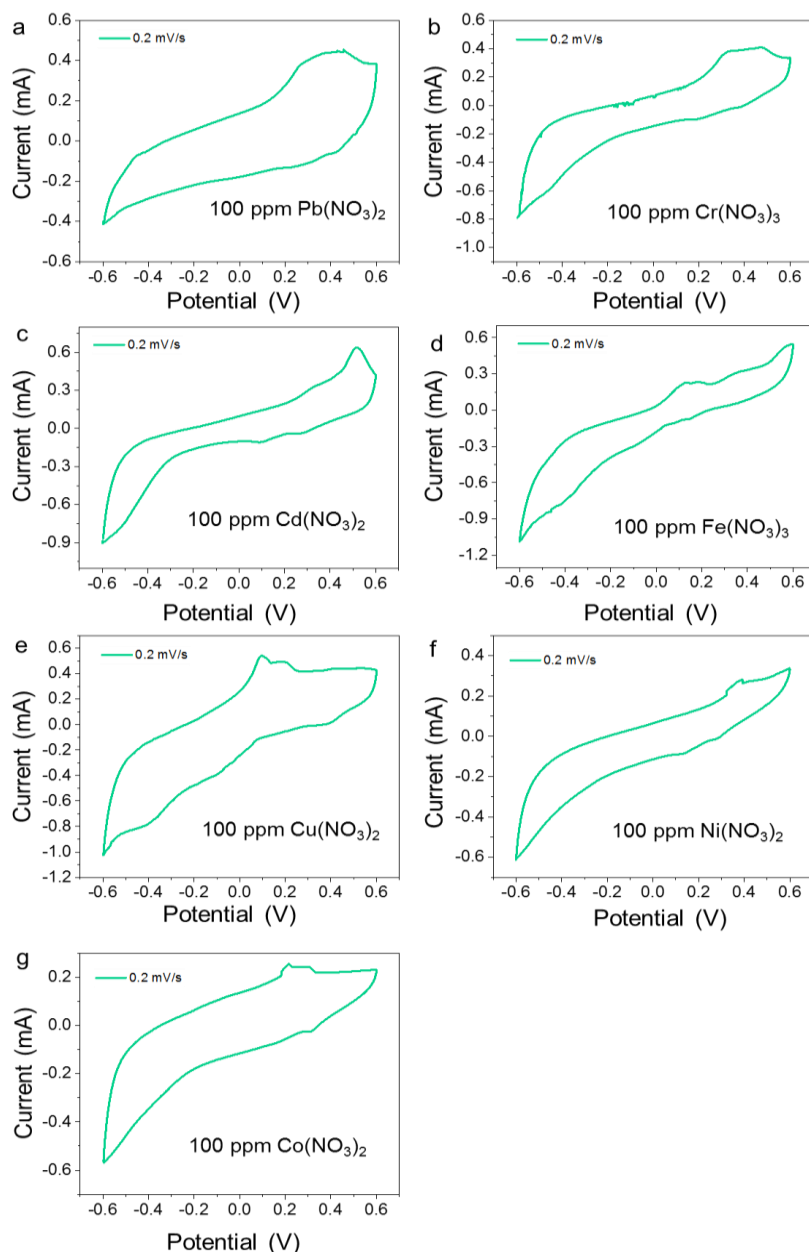


Figure S38. (a) CV curves at a scanning rate of 0.2 mV/s in 100 mg/L $\text{Pb}(\text{NO}_3)_2$ solutions, (b) CV curves at a scanning rate of 0.2 mV/s in 100 mg/L $\text{Cr}(\text{NO}_3)_3$ solutions, (c) CV curves at a scanning rate of 0.2 mV/s in 100 mg/L $\text{Cd}(\text{NO}_3)_2$ solutions, (d) CV curves at a scanning rate of 0.2 mV/s in 100 mg/L $\text{Fe}(\text{NO}_3)_3$ solutions, (e) CV curves at a scanning rate of 0.2 mV/s in 100 mg/L $\text{Cu}(\text{NO}_3)_2$ solutions, (f) CV curves at a scanning rate of 0.2 mV/s in 100 mg/L $\text{Ni}(\text{NO}_3)_2$ solutions, (g) CV curves at a scanning rate of 0.2 mV/s in 100 mg/L $\text{Co}(\text{NO}_3)_2$ solutions.

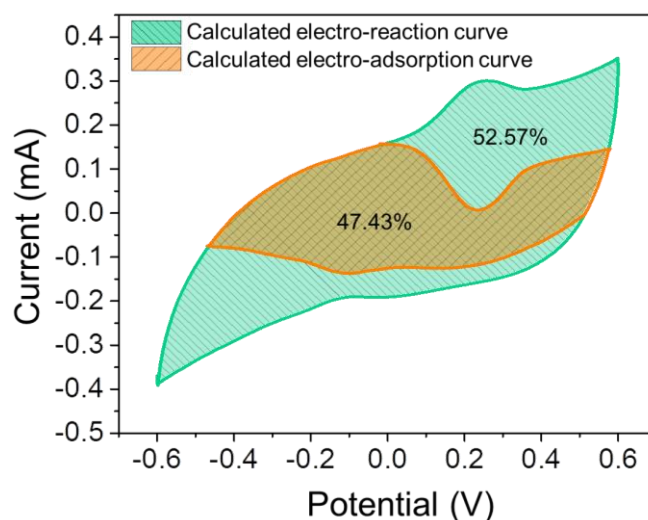


Figure S39. CV curves at a scanning rate of 0.2 mV/s in the multi-component solution containing all the seven metal nitrates (10 mg/L for each) and 100 mg/L NaCl.

The proportion of contribution of electro-adsorption and electro-reaction were calculated according to the Eq (12).¹¹

$$i(V) = k_1 v + k_2 v^{0.5} \dots \dots \dots (12)$$

where the i is the current (A), the v is the scanning rate (mV/s), k_1 and k_2 are constant values at a fixed potential. $k_1 v$ is related to the capacitive current raised from electro-adsorption and $k_2 v^{0.5}$ is related to electro-reaction.

CV curves at 0.2 and 0.5 mV/s have been measured, respectively. Based on the Eq (12), at a given potential P , two known different current values i_1 and i_2 are obtained at two scanning rates v_1 (0.2 mV/s) and v_2 (0.5 mV/s), thus obtaining a binary equations as follow:¹¹

$$i_1(P) = 0.2 k_1 + \sqrt{0.2} k_2 \dots \dots \dots (13)$$

$$i_2(P) = 0.5 k_1 + \sqrt{0.5} k_2 \dots \dots \dots (14)$$

k_1 and k_2 at P potential can be obtained by solving the abovementioned binary equations consisting Eq (13) and Eq (14). A CV cycle contains a series of potential

values, so a series of k_1 and k_2 values can be obtained. For the same material, k_1 and k_2 are fixed at a given potential. Therefore, at the scanning rate of 0.2 mV/s, the current derived from electro-adsorption can be obtained by the Eq (15).¹¹

$$i_{\text{electro-adsorption}}(V) = 0.2 k_1 \dots \dots \dots (15)$$

Where $i_{\text{electro-adsorption}}$ is the current derived from the electro-adsorption. These $i_{\text{electro-adsorption}}$ points can be linked to form a closed CV curve, which is the shaded part in Figure S39. The area of shaded part as a percentage of the area of the measured CV curve is the percentage of the contribution of the electro-adsorption. The rest is the electro-reaction contribution. The yellow shadow area is corresponding to the contribution of the electro-adsorption at 0.2 mV/s (Figure S39), which takes a proportion of 47.43%. The result demonstrates that electro-adsorption contributes 47.43% and the electro-reaction contributes 52.57%.

Table S1. Summary of properties of the materials.

Materials	$S_{\text{BET}}^{\text{a}}$ [m ² g ⁻¹]	$V_{\text{total}}^{\text{b}}$ [cm ³ g ⁻¹]	$V_{\text{Micropore}}^{\text{c}}$ [cm ³ g ⁻¹]	$V_{\text{macro\&meso}}^{\text{d}}$ [cm ³ g ⁻¹]
W ₁₈ O ₄₉ /Graphene	218	0.26	0.045	0.215
W ₁₈ O ₄₉ /C	181	0.23	0.065	0.165

^a Brunauer–Emmett–Teller surface area. ^b Calculated by single-point adsorption at a relative pressure of 0.98. ^c Calculated by V–t plot method. ^d Calculated by DFT method from the desorption isotherm linear plot.

548 Table S2. Summary of relative intensity ratios of all materials in Raman spectra.

Materials	Integral Area	Integral Area	I_D/I_G
	/ D band	/ G band	
W ₁₈ O ₄₉ /Graphene	244719.25158	103373.78731	2.37
W ₁₈ O ₄₉ /C	2142.78762	5060.35489	0.42
AC	312977.03653	141618.5685	2.21

549

550 Table S3. Elemental contents of the synthesized materials determined by XPS spectra.

Materials	C (%)	N (%)	O (%)	W (%)
W ₁₈ O ₄₉ /Graphene	64.09	3.03	24.43	8.44

551

552 Table S4. Comparison of the $W_{18}O_{49}$ /Graphene materials with the state-of-the-art

553 electrode materials.

Materials	Cell	voltage	NaCl	SAC	Desalination	Ref
	configuration	(V)	(mg/L)	(mg/g)	rate(mg/g/s) _{max}	
MoS ₂ -Graphene	HCDI	1.2	500	19	/	11
Na ₄ Ti ₉ O ₂₀	HCDI	1.4	250	23	/	12
Na-birnessite	HCDI	1.2	880	31	/	13
Fe-NC	CDI	1.2	500	36	/	1
MNPC	CDI	1.2	500	24	/	2
Na ₂ FeP ₂ O ₇	HCDI	1.2	1000	30	0.081	14
PHCs//HCs@MnO ₂	HCDI	1.2	500	30	0.130	15
PCNSs	CDI	1.1	500	15	0.017	16
Na _{0.44} MnO ₂	HCDI	1.2	585	31	0.066	17
SnS ₂ @GP	CDI	1.2	500	30	/	18
GPCSs	CDI	1.2	500	19	/	19
MoC@CNFA1	CDI	1.2	3000	37	0.200	20
rGO/TiO ₂	CDI	0.8	300	9	/	21
$W_{18}O_{49}$ /Graphene	CDI	1.2	1000	78	0.220	This work
$W_{18}O_{49}$ /Graphene	CDI	1.2	500	43	0.179	This work
$W_{18}O_{49}$ /Graphene	CDI	1.2	300	35	0.094	This work
$W_{18}O_{49}$ /Graphene	CDI	1.2	100	27	0.052	This work

554

555 Table S5. Removal efficiency after 120 min of capacitive adsorption in the complex
 556 binary-component solutions [metal nitrate (10 mg/L) and NaCl (100 mg/L)] at 1.2 V by
 557 ICP-OES tested.

	C_0 (mg/L)	C_t (mg/L)	Removal efficiency (%)
10 mg/L $\text{Pb}(\text{NO}_3)_2$ and 100 mg/L NaCl	10 (Pb^{2+})	0.031 (Pb^{2+})	99.7
10 mg/L $\text{Cr}(\text{NO}_3)_3$ and 100 mg/L NaCl	10 (Cr^{3+})	0.990 (Cr^{3+})	99.0
10 mg/L $\text{Cd}(\text{NO}_3)_2$ and 100 mg/L NaCl	10 (Cd^{2+})	0.113 (Cd^{2+})	98.9
10 mg/L $\text{Fe}(\text{NO}_3)_3$ and 100 mg/L NaCl	10 (Fe^{3+})	0.125 (Fe^{3+})	98.8
10 mg/L $\text{Co}(\text{NO}_3)_2$ and 100 mg/L NaCl	10 (Co^{2+})	0.142 (Co^{2+})	98.6
10 mg/L $\text{Ni}(\text{NO}_3)_2$ and 100 mg/L NaCl	10 (Ni^{2+})	0.134(Ni^{2+})	98.7
10 mg/L $\text{Cu}(\text{NO}_3)_2$ and 100 mg/L NaCl	10 (Cu^{2+})	0.131 (Cu^{2+})	98.7

558

Table S6. Removal efficiency after 120 min of capacitive adsorption in the complex binary-component solutions [metal nitrate (50 mg/L) and NaCl (100 mg/L)] at 1.2 V by ICP-OES tested.

	C_0 (mg/L)	C_t (mg/L)	Removal efficiency (%)
50 mg/L $\text{Pb}(\text{NO}_3)_2$ and 100 mg/L NaCl	50 (Pb^{2+})	0.079 (Pb^{2+})	99.8
50 mg/L $\text{Cr}(\text{NO}_3)_3$ and 100 mg/L NaCl	50 (Cr^{3+})	1.371 (Cr^{3+})	97.2
50 mg/L $\text{Cd}(\text{NO}_3)_2$ and 100 mg/L NaCl	50 (Cd^{2+})	5.006 (Cd^{2+})	90.0
50 mg/L $\text{Fe}(\text{NO}_3)_3$ and 100 mg/L NaCl	50 (Fe^{3+})	3.016 (Fe^{3+})	93.9
50 mg/L $\text{Co}(\text{NO}_3)_2$ and 100 mg/L NaCl	50 (Co^{2+})	3.386 (Co^{2+})	93.2
50 mg/L $\text{Ni}(\text{NO}_3)_2$ and 100 mg/L NaCl	50 (Ni^{2+})	4.800 (Ni^{2+})	90.4
50 mg/L $\text{Cu}(\text{NO}_3)_2$ and 100 mg/L NaCl	50 (Cu^{2+})	0.864 (Cu^{2+})	98.3

Table S7. Removal efficiency after 120 min of capacitive adsorption in the multi-component solution containing all the seven metal nitrates (10 mg/L for each) and 100 mg/L NaCl at a constant voltage of 1.2 V by ICP-OES tested.

Metal ions	C ₀ (mg/L)	C _t (mg/L)	Removal efficiency (%)
Pb ²⁺	10	0.024	99.7
Cr ³⁺	10	0.026	99.7
Cd ²⁺	10	0.032	99.6
Fe ³⁺	10	0.011	99.8
Co ²⁺	10	0.043	99.5
Ni ²⁺	10	0.017	99.8
Cu ²⁺	10	0.090	99.1
Na ⁺	100	74.00	26.0

Table S8. Removal efficiency after 120 min of capacitive adsorption in the multi-component solution containing all the seven metal nitrates (10 mg/L for each) and 500 mg/L NaCl at a constant voltage of 1.2 V by ICP-OES tested.

Metal ions	C ₀ (mg/L)	C _t (mg/L)	Removal efficiency (%)
Pb ²⁺	10	0.025	99.7
Cr ³⁺	10	0.019	99.8
Cd ²⁺	10	0.029	99.7
Fe ³⁺	10	0.010	99.9
Co ²⁺	10	0.016	99.8
Ni ²⁺	10	0.056	99.4
Cu ²⁺	10	0.032	99.6
Na ⁺	500	437.0	12.6

571 Table S9. Removal efficiency after 120 min of capacitive adsorption in the multi-
 572 component solution containing all the seven metal nitrates (50 mg/L for each) and 100
 573 mg/L NaCl at a constant voltage of 1.2 V by ICP-OES tested.

Metal ions	C ₀ (mg/L)	C _t (mg/L)	Removal efficiency (%)
Pb ²⁺	50	2.137	95.7
Cr ³⁺	50	4.807	90.3
Cd ²⁺	50	3.313	93.3
Fe ³⁺	50	1.210	97.5
Co ²⁺	50	3.756	92.4
Ni ²⁺	50	4.281	91.4
Cu ²⁺	50	0.580	98.8
Na ⁺	100	72.00	28.0

574

Table S10. Removal efficiency after 120 min of capacitive adsorption in the multi-component solution containing all the seven metal nitrates (50 mg/L for each) and 500 mg/L NaCl at a constant voltage of 1.2 V by ICP-OES tested.

Metal ions	C ₀ (mg/L)	C _t (mg/L)	Removal efficiency (%)
Pb ²⁺	50	1.527	96.9
Cr ³⁺	50	2.687	94.6
Cd ²⁺	50	1.731	96.5
Fe ³⁺	50	1.110	97.8
Co ²⁺	50	2.154	95.7
Ni ²⁺	50	2.182	95.6
Cu ²⁺	50	0.456	99.1
Na ⁺	500	441.5	11.7

Table S11. Heavy metal ions concentration of 20 cycles after 120 min of capacitive adsorption in the multi-component solution containing all the seven metal nitrates (10 mg/L for each) and 100 mg/L NaCl at a constant voltage of 1.2 V by ICP-OES tested.

Cycles`	1	5	10	15	20
Pb ²⁺ (mg/L)	0.024	0.024	0.036	0.075	0.024
Cr ³⁺ (mg/L)	0.026	0.021	0.031	0.021	0.043
Cd ²⁺ (mg/L)	0.032	0.035	0.038	0.032	0.037
Fe ³⁺ (mg/L)	0.011	0.030	0.053	0.074	0.070
Co ²⁺ (mg/L)	0.043	0.044	0.042	0.047	0.051
Ni ²⁺ (mg/L)	0.017	0.017	0.015	0.021	0.018
Cu ²⁺ (mg/L)	0.090	0.064	0.075	0.015	0.086

Table S12. Removal efficiency after 120 min of capacitive adsorption in the multi-component solution containing all the seven metal nitrates (10 mg/L for each) and 100 mg/L CaCl₂ at a constant voltage of 1.2 V by ICP-OES tested.

Metal ions	C ₀ (mg/L)	C _t (mg/L)	Removal efficiency (%)
Pb ²⁺	10	0.035	99.6
Cr ³⁺	10	0.022	99.7
Cd ²⁺	10	0.018	99.8
Fe ³⁺	10	0.050	99.5
Co ²⁺	10	0.072	99.3
Ni ²⁺	10	0.077	99.2
Cu ²⁺	10	0.035	99.6
Ca ²⁺	100	79.00	21.0

587 Table S13. Removal efficiency after 120 min of capacitive adsorption in the multi-
 588 component solution containing all the seven metal nitrates (10 mg/L for each) and 500
 589 mg/L CaCl₂ at a constant voltage of 1.2 V by ICP-OES tested.

Metal ions	C ₀ (mg/L)	C _t (mg/L)	Removal efficiency (%)
Pb ²⁺	10	0.097	99.0
Cr ³⁺	10	0.019	99.8
Cd ²⁺	10	0.016	99.8
Fe ³⁺	10	0.011	99.9
Co ²⁺	10	0.037	99.6
Ni ²⁺	10	0.031	99.7
Cu ²⁺	10	0.025	99.8
Ca ²⁺	500	449.0	10.2

590

591 Table S14. The area corresponding to the peak position of XPS.

	W ⁶⁺	W ⁶⁺	W ⁵⁺	W ⁵⁺	W ⁴⁺	W ⁴⁺
XPS	35.9	38.1	35.4	37.6	34.5	36.7
	eV/Area	eV/Area	eV/Area	eV/Area	eV/Area	eV/Area
W ₁₈ O ₄₉ /Graphene	21225	19382	7554	7230	4577	5808
Adsorbed Na	19463	19691	7461	7184	4488	5685
Adsorbed heavy metal ion	19866	18803	7781	13224	4388	2959

592

REFERENCES

1. Wang, G.; Yan, T.; Zhang, J.; Shi, L.; Zhang, D., Trace-Fe-enhanced capacitive deionization of saline water by boosting electron transfer of electro-adsorption sites. *Environ. Sci. Technol.* **2020**, *54*, 8411-8419.
2. Zhang, J.; Yan, T.; Fang, J.; Shen, J.; Shi, L.; Zhang, D., Enhanced capacitive deionization of saline water using N-doped rod-like porous carbon derived from dual-ligand metal-organic frameworks. *Environ. Sci-Nano.* **2020**, *7*, 926-937.
3. Liu, T.; Serrano, J.; Elliott, J.; Yang, X.; Cathcart, W.; Wang, Z.; He, Z.; Liu, G., Exceptional capacitive deionization rate and capacity by block copolymer-based porous carbon fibers. *Sci. Adv.* **2020**, *6*, eaaz0906.
4. Tan, G.; Lu, S.; Xu, N.; Gao, D.; Zhu, X., Pseudocapacitive behaviors of polypyrrole grafted activated carbon and MnO₂ electrodes to enable fast and efficient membrane-free capacitive deionization. *Environ. Sci. Technol.* **2020**, *54*, 5843-5852.
5. Wang, L.; Lin, S., Intrinsic tradeoff between kinetic and energetic efficiencies in membrane capacitive deionization. *Water. Res.* **2018**, *129*, 394-401.
6. Patel, S. K.; Qin, M.; Walker, W. S.; Elimelech, M., Energy efficiency of electro-driven brackish water desalination: Electrodialysis significantly outperforms membrane capacitive deionization. *Environ. Sci. Technol.* **2020**, *54*, 3663-3677.
7. Zhang, H.; Zhang, W.; Shen, J.; Li, Y.; Yan, X.; Qi, J.; Sun, X.; Shen, J.; Han, W.; Wang, L.; Li, J., Ag-doped hollow ZIFs-derived nanoporous carbon for efficient hybrid capacitive deionization. *Desalination.* **2020**, *473*, 114173.
8. Hawks, S. A.; Ramachandran, A.; Porada, S.; Campbell, P. G.; Suss, M. E.;

- 615 Biesheuvel, P. M.; Santiago, J. G.; Stadermann, M., Performance metrics for the
616 objective assessment of capacitive deionization systems. *Water. Res.* **2019**, *152*, 126-
617 137.
- 618 9. Lin, S., Energy efficiency of desalination: Fundamental insights from intuitive
619 interpretation. *Environ. Sci. Technol.* **2020**, *54*, 76-84.
- 620 10. Dykstra, J.; Porada, S.; van der Wal, A.; Biesheuvel, P. Energy consumption in
621 capacitive deionization—Constant current versus constant voltage operation. *Water. Res.*
622 **2018**, *143*, 367-375.
- 623 11. Han, J.; Yan, T.; Shen, J.; Shi, L.; Zhang, J.; Zhang, D., Capacitive deionization of
624 saline water by using MoS₂-graphene hybrid electrodes with high volumetric
625 adsorption capacity. *Environ. Sci. Technol.* **2019**, *53*, 12668-12676.
- 626 12. Zhou, F.; Gao, T.; Luo, M.; Li, H., Heterostructured graphene@Na₄Ti₉O₂₀
627 nanotubes for asymmetrical capacitive deionization with ultrahigh desalination capacity.
628 *Chem. Eng. J.* **2018**, *343*, 8-15.
- 629 13. Byles, B. W.; Hayes-Oberst, B.; Pomerantseva, E., Ion removal performance,
630 structural/compositional dynamics, and electrochemical stability of layered manganese
631 oxide electrodes in hybrid capacitive deionization. *ACS Appl. Mater. Inter.* **2018**, *10*,
632 32313-32322.
- 633 14. Kim, S.; Lee, J.; Kim, C.; Yoon, J., Na₂FeP₂O₇ as a novel material for hybrid
634 capacitive deionization. *Electrochim. Acta.* **2016**, *203*, 265-271.
- 635 15. Wang, S.; Wang, G.; Wu, T.; Li, C.; Wang, Y.; Pan, X.; Zhan, F.; Zhang, Y.; Wang,
636 S.; Qiu, J., Membrane-free hybrid capacitive deionization system based on redox

637 reaction for high-efficiency NaCl removal. *Environ. Sci. Technol.* **2019**, 53, 6292-6301.

638 16. Wu, T.; Wang, G.; Dong, Q.; Zhan, F.; Zhang, X.; Li, S.; Qiao, H.; Qiu, J., Starch
639 derived porous carbon nanosheets for high-performance photovoltaic capacitive
640 deionization. *Environ. Sci. Technol.* **2017**, 51, 9244-9251.

641 17. Lee, J.; Kim, S.; Kim, C.; Yoon, J., Hybrid capacitive deionization to enhance the
642 desalination performance of capacitive techniques. *Energy. Environ. Sci.* 2014, 7, 3683-
643 3689.

644 18. Wen, X.; Zhao, M.; Zhang, M.; Fan, X.; Zhang, D., Efficient capacitive
645 deionization of saline water by an integrated tin disulfide nanosheet@graphite paper
646 electrode via an in situ growth strategy. *ACS Sustain. Chem. Eng.* **2020**, 8, 1268-1275.

647 19. Wang, H.; Yan, T.; Shen, J.; Zhang, J.; Shi, L.; Zhang, D., Efficient removal of
648 metal ions by capacitive deionization with straw waste derived graphitic porous carbon
649 nanosheets. *Environ. Sci-Nano.* **2020**, 7, 317-326.

650 20. Liu, Y.; Zhang, Y.; Zhang, Y.; Zhang, Q.; Gao, X.; Dou, X.; Zhu, H.; Yuan, X.; Pan,
651 L., MoC nanoparticle-embedded carbon nanofiber aerogels as flow-through electrodes
652 for highly efficient pseudocapacitive deionization. *J. Mater. Chem. A.* **2020**, 8, 1443-
653 1450.

654 21. El-Deen, A. G.; Choi, J.-H.; Kim, C. S.; Khalil, K. A.; Almajid, A. A.; Barakat, N.
655 A. M., TiO₂ nanorod-intercalated reduced graphene oxide as high performance
656 electrode material for membrane capacitive deionization. *Desalination.* **2015**, 361, 53-
657 64.